

## Centaur Nuclei: Sizes, Shapes, Spins, and Structure\*

Y. R. FERNÁNDEZ <sup>1</sup> M. W. BUIE <sup>2</sup> P. LACERDA <sup>3,4</sup> AND R. MARSCHALL <sup>5</sup>

<sup>1</sup>*Department of Physics, University of Central Florida, Orlando, USA*

<sup>2</sup>*Southwest Research Institute, Boulder, USA*

<sup>3</sup>*Instituto de Astrofísica e Ciências do Espaço, Universidade de Coimbra, Coimbra, Portugal*

<sup>4</sup>*Instituto Pedro Nunes, Coimbra, Portugal*

<sup>5</sup>*Centre National de la Recherches Scientifique, Observatoire de la Côte d’Azur, Nice, France*

### ABSTRACT

We present a wide-ranging but in-depth analysis of Centaurs, focusing on their physical and structural aspects. Centaurs, originating from the Scattered Disk and Kuiper Belt, play a crucial role in our understanding of Solar System evolution. We first examine how biases in discovery and measurement affect our understanding of the Centaur size distribution. In particular we address the strong dependence of the census on perihelion distance and the broad distribution of Centaur geometric albedos. We explore the rotational characteristics derived from lightcurves, revealing a diverse range of spin rates and photometric variabilities, with most Centaurs showing low amplitude lightcurves, suggesting near-spherical shapes. Additionally, we investigate the relationships between Centaur orbital parameters, surface colors, and physical properties, noting a lack of correlation between rotational dynamics and orbital evolution. We also address the influence of sublimation-driven activity on Centaur spin states, and the rarity of contact binaries. We then discuss some observational and modeling limitations from using common observations (e.g. visible or infrared photometry) to determine diameters and shapes. Following that, we give some points on understanding how Centaur diameters and shapes can reveal the ‘primitive’ nature of the bodies, emphasizing the important role occultation observations play. We also then assess how the Centaur size distribution we see today has been influenced by the collisions in both the primordial Kuiper Belt and in the subsequent Scattered Disk. Finally, we end the chapter with a short narrative of future prospects for overcoming our current limitations in understanding Centaur origins and evolution.

### 1. INTRODUCTION

As described by other works in this volume (e.g., Chapters 1 and 7, [K. Volk et al. 2025](#); [R. Kokotanekova et al. 2025](#)), the current sizes, shapes, spin states, and structures of Centaurs are manifestations of the evolutionary processes that they have suffered since the original icy planetesimals were first accreted (see, e.g., Chapter 2, [A. Johansen et al. 2025](#)). In principle, if we were to

Email: yan@ucf.edu

\* This is an adapted, preprint version of the document that appears as Chapter 4 in the book *Centaurs* (K. Volk, M. Womack, J. Steckloff, Eds.), IOP Publishing, Bristol, UK, pp. 4-1 to 4-27, DOI 10.1088/2514-3433/ada267ch4 (2025).

know these physical properties of the entire Centaur population, and of the small-body groups that the Centaurs are related to, then we would have useful constraints that would have to be matched by any model purporting to explain the evolution.

Centaurs in particular play a unique role in our quest to understand Solar System evolution, since they come from the Scattered Disk (i.e., as Scattered Disk Objects, SDOs) and the Kuiper Belt, and since many of them end up as Jupiter-family comets (JFCs); see, e.g., [M. J. Duncan & H. F. Levison \(1997\)](#); [M. Duncan et al. \(2004\)](#); [K. Volk & R. Malhotra \(2008\)](#) and Chapter 3 ([R. P. Di Sisto et al. 2025](#)). A broad objective with studying Centaur physical properties is thus to contextualize what we see among the SDOs and JFCs. Part of this objective is an understanding of just if and how the Centaurs change before and during the dynamical cascade from the Scattered Disk, and what happens to the Centaurs in the (typically) few  $10^6$  yr of their residence in the giant-planet region.

While there is much ongoing work to understand the physical properties of Centaurs, a murky fog hinders us in several ways. First, as with many groups of small bodies in the Solar System, the characterization of Centaurs lags somewhat behind their discovery. There are many Centaurs with only minimal characterization. Second, the discovery of Centaurs itself has biases, so even if we were characterizing all known Centaurs well, there would still be gaps in our knowledge because we are simply ignorant of many of the faintest and smallest objects in the population. Third, the techniques that we use to measure Centaur brightnesses and thereby extract physical properties have their own set of limitations. All of these problems conspire to bias our picture of what we know about Centaur ensemble properties, and eventually they must be all well understood if we are to properly interpret our data.

In this chapter we focus on two themes that touch on these issues. (1) What are the current constraints on Centaur physical properties, and how might limitations in our measurement techniques be biasing those results? (2) What is the context of Centaurs in terms of primitive-body evolution in the Solar System?

## 2. SIZE DISTRIBUTION

Much of the physics of this topic is discussed in Chapter 7 ([R. Kokotanekova et al. 2025](#)), so we describe a few statistical points here. A very basic look at the current absolute magnitude ( $H$ ) distribution of the known Centaurs is shown in Figure 1. We extracted all asteroid entries in the JPL Horizons database (as of 2023 November 21) that had  $q > 5.203$  au (i.e., Jupiter’s orbital semimajor axis  $a_J$ ) and  $a < 30.1$  au (i.e., Neptune’s orbital semimajor axis  $a_N$ ), but excluding objects that are (or could be) from different source regions: Jovian and Neptunian Trojans, parabolic and hyperbolic objects, and nine additional objects with inclinations above  $80^\circ$ . This left 308 Centaurs. We note that this  $a_N$  cutoff in the Centaur definition does introduce some bias in the distant Centaurs since there is no real physical/dynamical break here between Scattered Disk and Centaur region; e.g. (523746) 2014 UT<sub>114</sub> with  $a = 30.09$  au makes our cut, but (309239) 2007 RW<sub>10</sub> with  $a = 30.16$  au does not. We also note that even if the high-inclination/retrograde Centaurs are indeed from the Scattered Disk anyway (see, e.g., [F. Namouni & M. H. M. Morais 2020](#)) this is a small number and does not affect the point we are making here.

The magnitude distribution of those 308 Centaurs are represented by the thick solid line in the Figure 1. The curves with other linestyles/colors show the distribution broken up into perihelion bins, as listed in the figure’s legend. We decided to create bins where approximately equal number of Centaurs would be in each one. The idea is to show that the discovery rates very strongly depend

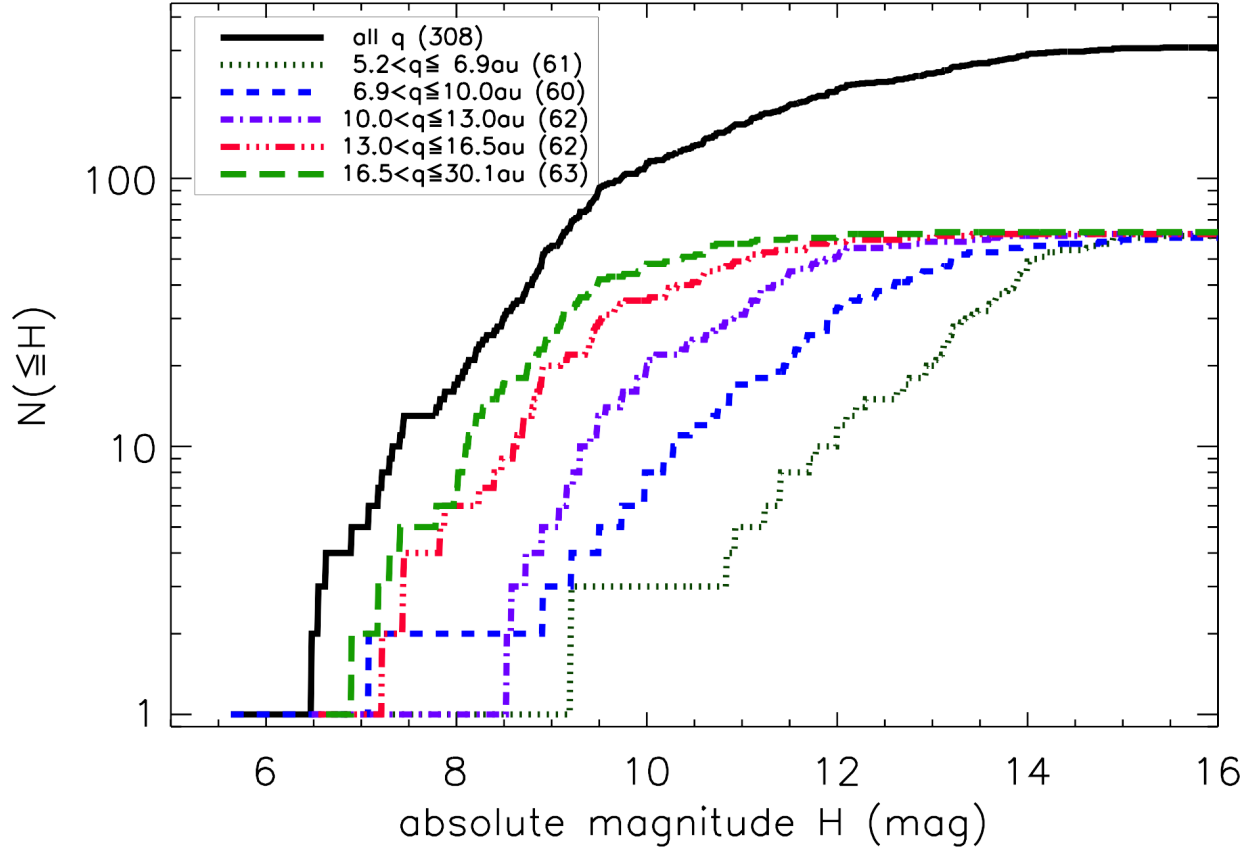


**Figure 1.** Cumulative magnitude distribution (CMD) of known asteroidal Centaurs. All objects (as described in the text) are in the thick black line. The other five thick linestyles with color show CMDs for various perihelion ( $q$ ) bins, tuned so that each bin has approximately the same number of Centaurs. There are very strong differences in the five curves indicating that the completion of the Centaur census does not extend to very faint magnitudes yet.

on how close the Centaurs come to our telescopes here in the inner Solar System. For the smallest perihelion bin (green dotted line), the magnitude distribution seems to be a single power law that turns over due to lack of detected objects around  $H = 14$ . In contrast, the other curves are less straight and of course also turn over at brighter values of  $H$ . The most distant bin, the light green dashed line, has a turn over about 5 full magnitudes brighter than the closest bin. One could argue from this that we are only really confident in our census of the Centaurs down to about  $H = 9$ , and we certainly have not yet discovered enough Centaurs in the  $H = 9$  to 14 range to permit characterizing the population in this size range without large corrections due to discovery biases.

Another demonstration of the aforementioned perihelion effect is shown in Figure 2, which plots the discovery time versus a Centaur's  $H$ . The color coding here is the same as in the previous figure. For the Centaurs that are presumably easier to discover, i.e. those in the closest perihelion bin (green squares), there is some indication that we have discovered all or nearly all of the relatively large Centaurs ( $H \approx 13$  and brighter). In the last few years, the only such Centaurs discovered in that bin are around  $H = 13$  to 15. This is true even though clearly the sky surveys are still capable of finding brighter Centaurs, since those are in fact being found in the more distant perihelion bins.

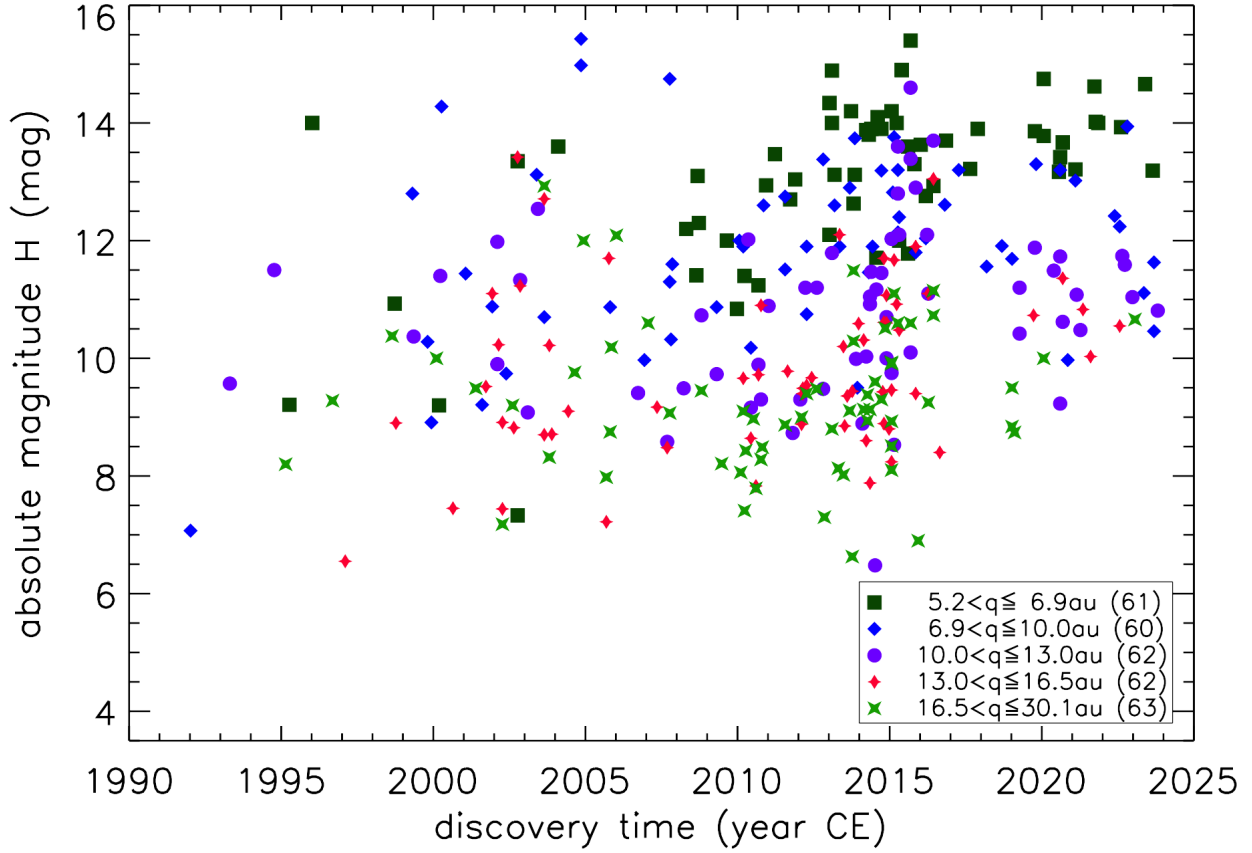


**Figure 2.** Scatter plot of when asteroidal Centaurs of various  $q$  and  $H$  were discovered. Color coding and perihelion binning match that in Figure 1.

Interestingly, no Centaur brighter than about  $H = 8.7$  has been discovered since late 2016 (7 years ago at time of writing).

The fundamental property that we wish to understand is the size distribution, not the magnitude distribution, and so the geometric albedo is required to make the conversion. (See, e.g., [P. Pravec & A. W. Harris \(2007\)](#) for a definition of this albedo.) With JFCs, the spread of albedos seems to be fairly limited (see, e.g., [P. L. Lamy et al. 2004](#)), but this is not the case for Centaurs. Using a recent compilation of outer Solar System albedos by [T. Müller et al. \(2020\)](#), we make use of 42 Centaur albedos in their Table 7.1. (The table itself lists 55 Centaurs, but here we exclude 3 active comets for which the nucleus albedo may be difficult to get (29P, 167P, and C/2011 KP36) as well as 10 other objects that [T. Müller et al. \(2020\)](#) included as Centaurs even though their perihelia are smaller than  $a_J$ .) A scatter plot of those 42 albedos is shown in the top of Figure 3. The color coding for perihelion bins is again the same as the previous figures. There is no trend of albedo with diameter, and no significant difference between the albedos in any perihelion bin (via a check of the Kolmogorov-Smirnov (KS) test). At the moment, if one were to assume that albedo is controlled by the surface evolution of the Centaur (see Chapter 5, Chapter 6, Chapter 7, Chapter 8; [N. Peixinho et al. 2025](#); [K. Mandt et al. 2025](#); [R. Kokotanekova et al. 2025](#); [J. Bauer et al. 2025](#)), there is apparently no indication that surfaces of Centaurs with smaller  $q$  have evolved differently than those of the Centaurs farther out. This might be simply a manifestation of the fact that Centaurs do jostle

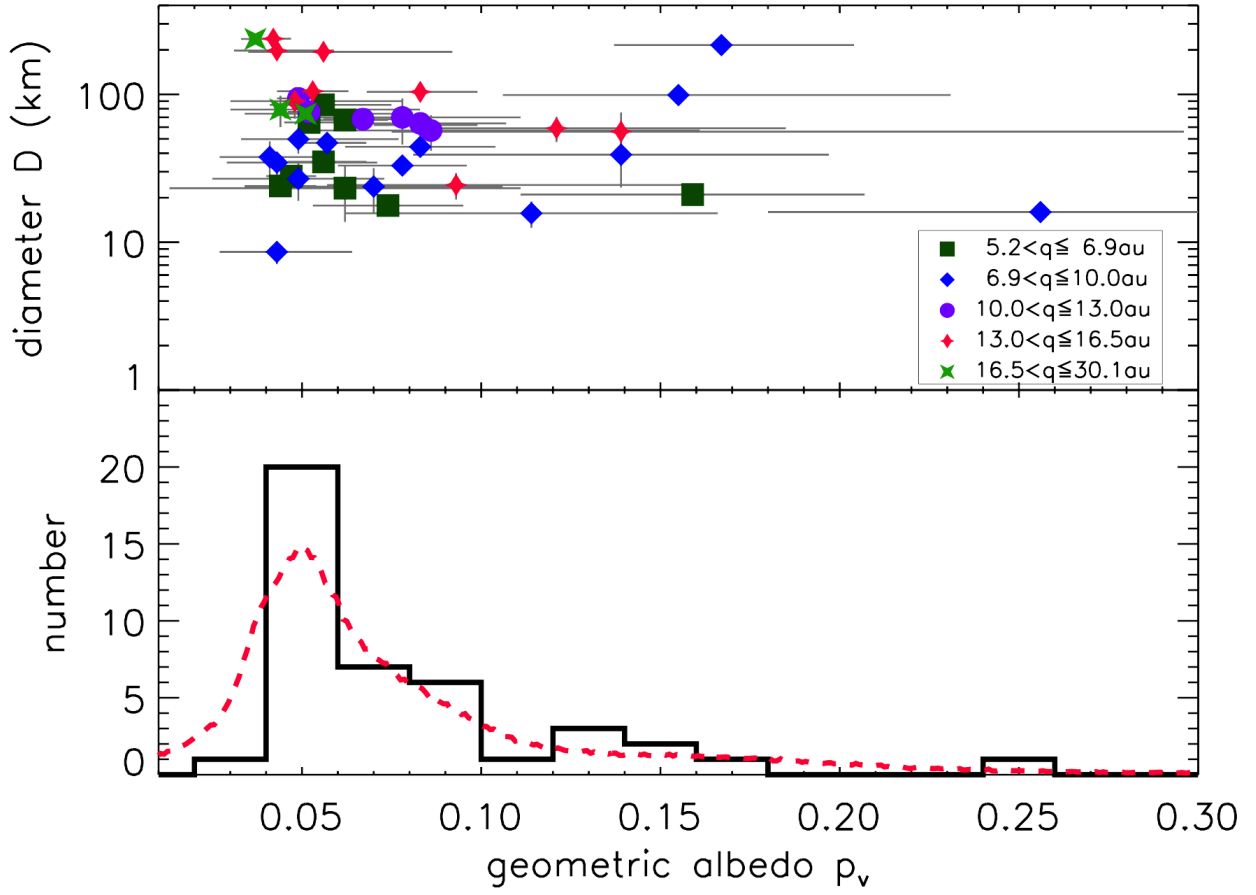


**Figure 3.** Top: Scatter plot of 42 Centaur diameters  $D$  and geometric albedos  $p_v$  as summarized by T. Müller et al. (2020). Color coding matches that in Figures 1 and 2. Bottom: Histogram of those 42 albedos. The red dashed curve is our estimate of the albedo probability density function (PDF) based on the given albedos. We estimated the PDF by generating simulated albedos based on the measured values and their uncertainties.

toward and away from the Sun in the Centaur region, even if there is an overall trend of the Centaurs (at least the ones that survive to become JFCs) slowly moving inward (M. Duncan et al. 2004; W. C. Fraser et al. 2024).

Given the absence of a strong trend of albedo with perihelion or semimajor axis, we will take the current albedo distribution for those 42 Centaurs as being representative of the population as a whole, and use it as a probability density function (PDF) in order to explore what the size distribution might be as derived from the  $H$  distribution. In other words, since we have albedos for less than 1/7 of the Centaurs (42 out of 308), the conversion requires assuming an albedo distribution. The histogram of those 42 albedos is shown in the bottom panel of Figure 3. We estimated a PDF from those 42 measurements and their error-bars by simulating 10,000 albedo distributions Monte Carlo-style. The result is the red dashed curve in the bottom plot of Figure 3. Note that this is not a fit to the albedo distribution, simply an empirical assessment of what the true underlying distribution might be.

Using this PDF, we then simply ran 10,000 simulations that each created a size distribution from the magnitude distribution by randomly extracting an albedo for each object according to the probability density. We then fit a power-law to each cumulative size distribution with diameters between 100

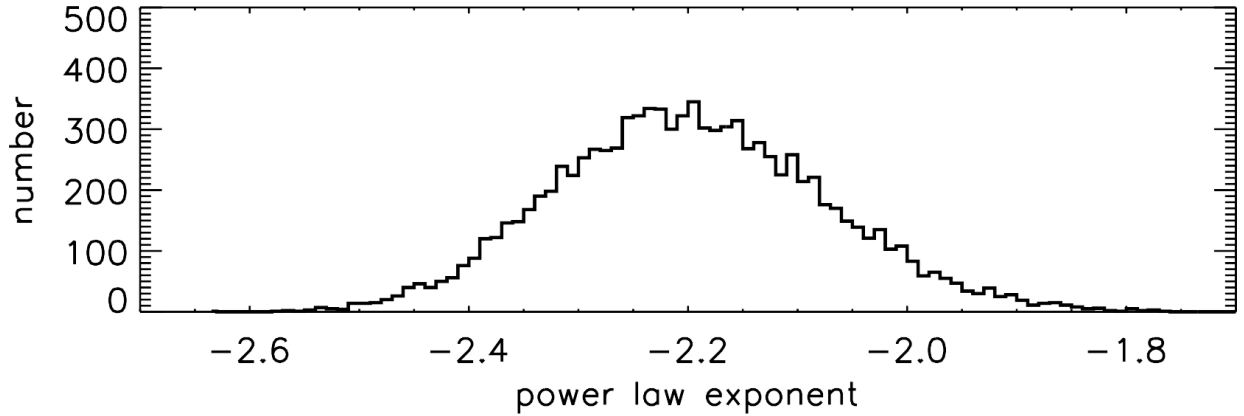


**Figure 4.** Distribution of power-law slopes from our simulation of 10000 cumulative size distributions created as described in the text. While the most likely result of our particular fit scheme is around  $-2.2$ , there is a wide range of other possible exponents, and this must be taken into account when interpreting the Centaur size distribution. Note that we are not claiming a value for the actual Centaur size distribution, we are merely demonstrating that whatever power-law is produced has appreciable uncertainty.

and 200 km. This range was chosen as one for which the distribution seems to follow a single power-law; i.e. it made the fitting seem sensible. The distribution of those 10000 power-law exponents is shown in Figure 4. While there is a most-likely result near a power-law exponent of  $-2.2$ , there is a reasonable probability of getting an exponent that is well off from that answer. We emphasize that the main point here is not the actual value of the exponent, but rather that until a higher fraction of the Centaur diameters and albedos (not just their  $H$  magnitudes) have actually been measured, there is intrinsic uncertainty in any characterization of the Centaur size distribution. This has ramifications for any attempt to use a physical model to explain such a size distribution or to explain how Centaurs fit into the SDO and JFC size distributions. This is above and beyond other problems that could make such hypothesizing difficult – e.g. the fact that there is almost no overlap between the known JFC diameters and the known Centaur diameters.

It can be argued that the size distribution is not actually the most fundamental property we might use to gauge formation and evolutionary processes. Rather in some contexts the mass distribution might be more important. This is currently even more fraught than the size assessment is since to go from size to mass requires a density, and we have precious little info on the densities, porosities, and overall structure of the Centaurs (see 3.6 below, and Chapters 9 and 12; [A. Sickafoose et al. 2025](#); [M. Hirabayashi et al. 2025](#)).

### 3. SHAPE AND SPIN DISTRIBUTIONS

Determining the shapes and spins of Centaurs involves studying their lightcurves, which record periodic oscillations in brightness over time. Well sampled lightcurves are processed to extract rotational properties: the period,  $P$ , and the full range of photometric variation,  $\Delta m$ . The former corresponds to the spin period, while the latter constrains the shape of individual objects. If measured at different observing geometries, time series data can be inverted to extract more precise shapes and spin pole orientations. In some cases, under favorable observing geometries, lightcurves can also reveal whether the object has multiple components (bilobed shape as the nucleus 67P, or two separate



components as KBO Arrokoth). The distributions of rotational properties are useful for comparing different populations when trying to decode evolutionary links between them.

Other techniques exist to decipher the shapes of Centaurs. For bright objects, adaptive optics systems on ground-based telescopes can also be used to estimate their shapes and dimensions. Stellar occultations are a powerful technique to constrain shapes, capable of achieving extraordinary resolution on chords across the sky-projected cross-section of individual objects. These techniques are often complementary.

The Asteroid Lightcurve Database (B. D. Warner et al. 2009) currently includes lightcurve properties, spin period and photometric range, for 16 Centaurs. Of those, 7 have been observed at more than one observing geometry, revealing changing variability. Table 1 summarises the known Centaur rotational properties, listed together with other orbital, physical and surface parameters. Figures 5-11 highlight a few aspects of data discussed in this chapter.

### 3.1. *Period and $\Delta m$ distributions*

Figures 5 and 6 show histograms and cumulative distributions of spin frequency and lightcurve variability. Even though the period is often easier to grasp, frequency is the more relevant physical quantity; we will refer to both interchangeably. Six of the 16 Centaurs cluster between 2.5 and 3 rotations per day ( $P \sim 9$  hr) near the center of the distribution. A long tail extends to much slower rotations, with 3 objects spinning slower than  $P = 24$  hr and Centaur 2013 XZ8 spinning with  $P \sim 88$  hr. The two fastest rotators are Chiron and 2002 GZ32 with periods near 6 hr.

The  $\Delta m$  distribution is skewed towards low values, with roughly half the Centaurs within  $\Delta m < 0.2$  mag. At the opposite end of the distribution, Bienor is the most variable object at  $\Delta m = 0.75$  mag. As of yet no Centaurs display the extreme variability ( $\Delta m > 0.9$  mag) characteristic of extreme bilobed or compact binary shapes (although it is possible that there is a bias against discovering such objects, since perhaps the large lightcurve amplitude means it is less likely for such objects to be seen at follow-up observations right after discovery). We discuss binarity in more detail below. Another bias against discovery highly variable objects is that larger objects, which are easier to detect, will tend to be more spherical (although high- $\Delta m$  Bienor is the 4th largest object in Table 1.)

Figure 7 compares the spin rate distribution of Centaurs with different dynamical families of transneptunian objects. We use the two-sample KS test<sup>6</sup> to compare the Centaurs with the other classes of objects. Cold Classical have the least compatible spin distribution with the Centaurs ( $p_{\text{KS}}$ -value of 0.05). The KS-test does not rule that Centaur spins come from the same distribution as Plutinos ( $p_{\text{KS}} = 0.15$ ), Scattered Disk objects ( $p_{\text{KS}} = 0.33$ ) or Hot Classicals ( $p_{\text{KS}} = 0.44$ ). However, the sample sizes are small so more data is needed before strong conclusions can be made. A similar exercise comparing the max  $\Delta m$  distributions of Centaurs and the same transneptunian dynamical families shows no discernible differences, with  $p_{\text{KS}} > 0.66$  in all cases.

### 3.2. *Relation to orbits*

Centaurs display no obvious relation between orbital parameters (perihelion distance, orbital eccentricity and inclination) and lightcurve properties. To zeroth order, this suggests that the processes responsible for the orbital evolution and the spin evolution are unrelated. One possible exception is that higher perihelion objects have lower  $\Delta m$  lightcurves (although again there may be some bias

<sup>6</sup> We used the implementation provided in Python module `scipy.stats.ks_2samp`.

Table 1. Known Centaur Rotational Properties

Centaur	Lightcurve Period <sup>a</sup> [hr]	Abs.					Mag. $B - R$		Surface Geometric Albedo	Diameter $D$ [km]	Notes <sup>b</sup>
		Min. $\Delta m$ [mag]	Max. $\Delta m$ [mag]	$q$ [au]	$e$ [deg]	$i$ [deg]	$H$ [hr]	Color [mag]			
2060 Chiron (1977 UB)	5.92	0.04	0.09	8.55	0.376	6.9	6.56	1.01	0.16 $\pm$ 0.03	218 $\pm$ 20	U3, C, R?
5145 Pholus (1992 AD)	9.98	0.15	0.6	8.67	0.573	24.7	7.64	1.97	0.16 $\pm$ 0.08	99 $\pm$ 15	U3
8405 Asbolus (1995 GO)	8.94	0.32	0.55	6.88	0.619	17.6	9.19	1.228	0.06 $\pm$ 0.02	85 $\pm$ 9	U3
10199 Chariklo (1997 CU26)	7.00		0.11	13.14	0.168	23.4	6.65	1.299	0.04 $\pm$ 0.01	248 $\pm$ 18	U2, R
31824 Elatus (1999 UG5)	26.82		0.1	7.22	0.386	5.3	10.42	1.672	0.05 $\pm$ 0.03	50 $\pm$ 10	U2
32532 Thereus (2001 PT13)	8.34	0.16	0.38	8.50	0.199	20.4	9.29	1.19	0.07 $\pm$ 0.02	74 $\pm$ 17	U3
52872 Okyrhoe (1998 SG35)	9.72	0.07	0.4	5.82	0.305	15.7	11.23	1.237	0.06 $\pm$ 0.02	36 $\pm$ 1	12.17, U2
54598 Bienor (2000 QC243)	9.14	0.08	0.75	13.20	0.203	20.7	7.69	1.158	0.04 $\pm$ 0.02	198 $\pm$ 7	U3
60558 Echeclus (2000 EC98)	26.80		0.24	5.84	0.457	4.3	9.55	1.376	0.05 $\pm$ 0.02	65 $\pm$ 2	U2, C
83982 Crantor (2002 GO9)	13.94		0.14	14.1	0.274	12.8	9.17	1.864	0.12 $\pm$ 0.06	59 $\pm$ 12	19.34, U1
95626 (2002 GZ32)	5.8		0.08	18.01	0.219	15.0	7.39	1.199	0.04 $\pm$ 0.01	237 $\pm$ 8	U3
136204 (2003 WL7)	8.24		0.05	14.92	0.258	11.2	8.73	1.23	0.05 $\pm$ 0.01	105 $\pm$ 7	S, U2-
145486 (2005 UJ438)	8.32		0.13	8.22	0.532	3.8	10.89	1.64	0.24 $\pm$ 0.12	16 $\pm$ 2	A, U2-
250112 (2002 KY14)	8.50	0.09	0.13	8.62	0.314	19.5	9.74	1.75	0.12 $\pm$ 0.09	43 $\pm$ 6	U2
459865 (2013 XZ8)	87.74		0.26	8.42	0.369	22.6	9.53	1.17		69 $\pm$ 35 <sup>c</sup>	U2
471931 (2013 PH44)	22.16		0.15	15.57	0.213	33.5	9.38			74 $\pm$ 37 <sup>c</sup>	A, U1

NOTE—Lightcurve properties taken from Lightcurve Database (B. D. Warner et al. 2009), updated October 2023. Diameters and albedos come from Herschel (S. Fornasier et al. 2013; R. Duffard et al. 2014), or NEOWISE (A. K. Mainzer et al. 2019) surveys; the least uncertain of the two measurements is taken when they agree within  $1\sigma$ , otherwise the mean is shown. Colours taken from N. Peixinho et al. (2012) and S. C. Tegler et al. (2016).

<sup>a</sup>Lightcurve period, where all are double peaked except where indicated in notes.

<sup>b</sup>“U( $x$ )-” is the quality of the lightcurve from  $x = 1$  (worse) to  $x = 3$  (best) and “\_” is a half-step, “S” indicates a single-peaked period is given, “A” indicates ambiguity between double-peaked and single-peaked period, and a number indicates another possible period. “C” indicates cometary activity, “R” means rings detected (followed by “?” if unconfirmed).

<sup>c</sup>An albedo of 0.057 is assumed to calculate diameter from  $H$  for last two rows.



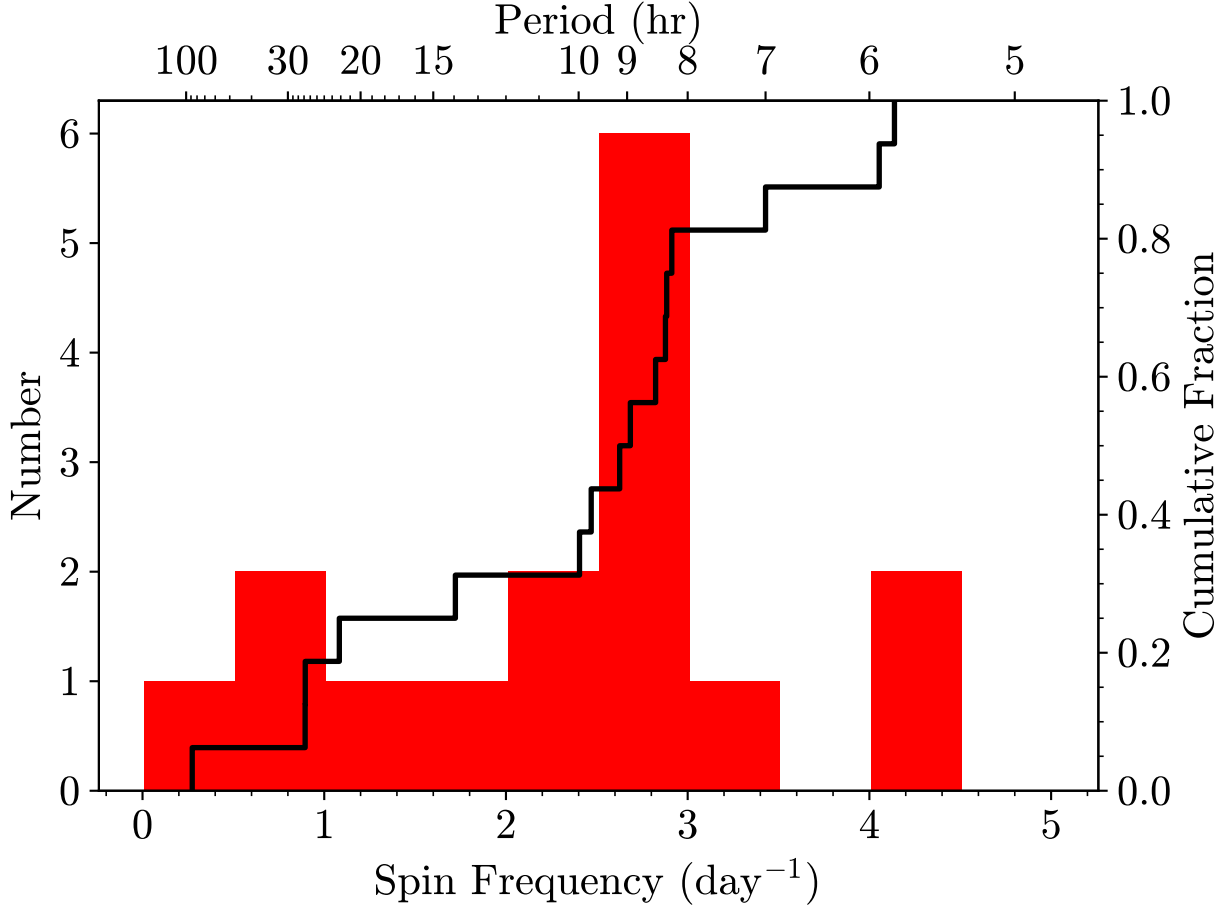


**Figure 5.** Centaur spin rate distribution. Cumulative distribution (solid black line) is plotted on the right vertical axis.

against recovering such objects in the first place). Since Centaur activity correlates inversely with perihelion distance, this suggests a possible link between shape and activity. We discuss this possibility below. However, it would be interesting to study whether close approaches to giant planets can significantly modulate Centaur spins and shapes.

### 3.3. Relation to surface properties

The surface colors of Centaurs and small Kuiper Belt objects span a broad range from a solar  $B - R \approx 1$  mag to a very red  $B - R \approx 2$  mag. Furthermore, the color distribution appears bimodal, with a gap at  $B - R \sim 1.5$  mag (N. Peixinho et al. 2012, 2020). The reason for this surface color bimodality is unclear (N. Peixinho et al. 2020). An initial explanation based on collisional resurfacing of radiation reddened surface with freshly excavated, neutrally colored material (J. Luu & D. Jewitt 1996) was ruled out (J. X. Luu & D. C. Jewitt 1998; P. Thébault 2003). Cometary activity may also cause the resurfacing, affecting the colors of Centaurs and causing the bimodality (A. Delsanti et al. 2004). Indeed, all active Centaurs but one<sup>7</sup> occupy the bluer of the two color clumps. If low level, undetectable activity is present, this can also be due to intrinsically bluer coma dust diluting

<sup>7</sup> The exception is 166P ( $q = 8.6$  au,  $Q = 19.2$  au, unknown rotational properties) which falls in neither the blue nor the red clump

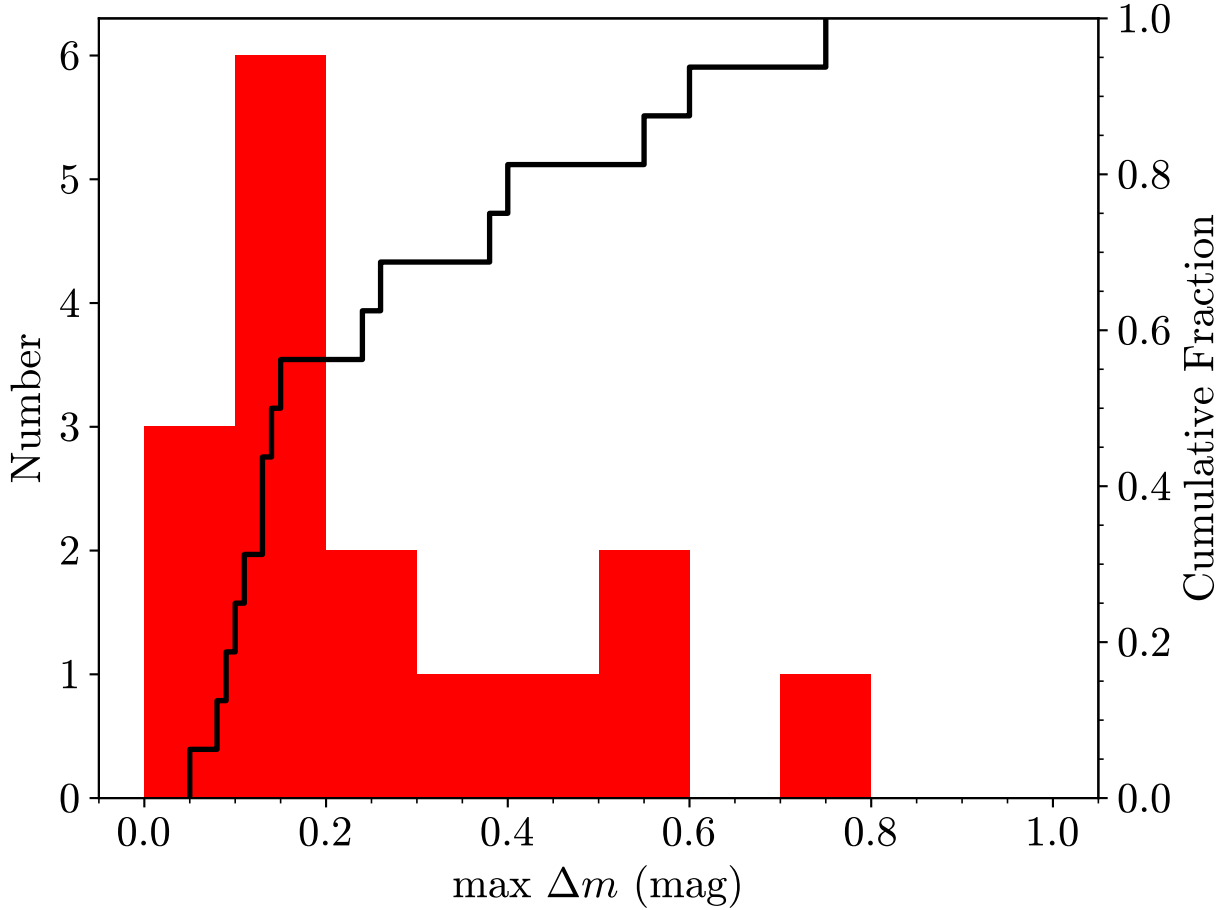


**Figure 6.** Distribution of maximum lightcurve variability for Centaurs. Cumulative distribution (solid black line) is plotted on the right vertical axis.

the redder color of the nucleus, or simply to nongeometric scattering in optically small particles dominating the coma and making it appear bluer (D. Jewitt 2009). Another possibility is that the bimodality stems from a composition gradient with heliocentric distance in the planetesimal disk from which the Centaurs originate (e.g. I. Wong & M. E. Brown 2017; P.-Y. Liu & W.-H. Ip 2019). Basically, depending on where a Centaur progenitor actually formed with respect to the condensation lines of various red species, a surface could evolve differently due to the subsequent radiation and thermal processing, perhaps leading to the discontinuity of colors that we see today.

In any case these processes do not appear to correlate with the rotational properties of Centaurs, as shown in Figure 8. The different types of surfaces scatter across the entire range of observed spin frequencies. The red clump of Centaurs concentrates at low  $\Delta m$ , with the exception of Pholus, but this may be a small number fluctuation. An interesting observation not related to rotational properties is that blue Centaurs are darker. This is also seen in other outer Solar System populations (P. Lacerda et al. 2014b).

### 3.4. Relation to Centaur size

Figure 9 (left panel) plots Centaur size against spin frequency and period. Smaller Centaurs ( $D < 100$  km) span a wide range of observed spin frequencies, from 0.5 to 3 rotations per day, with a

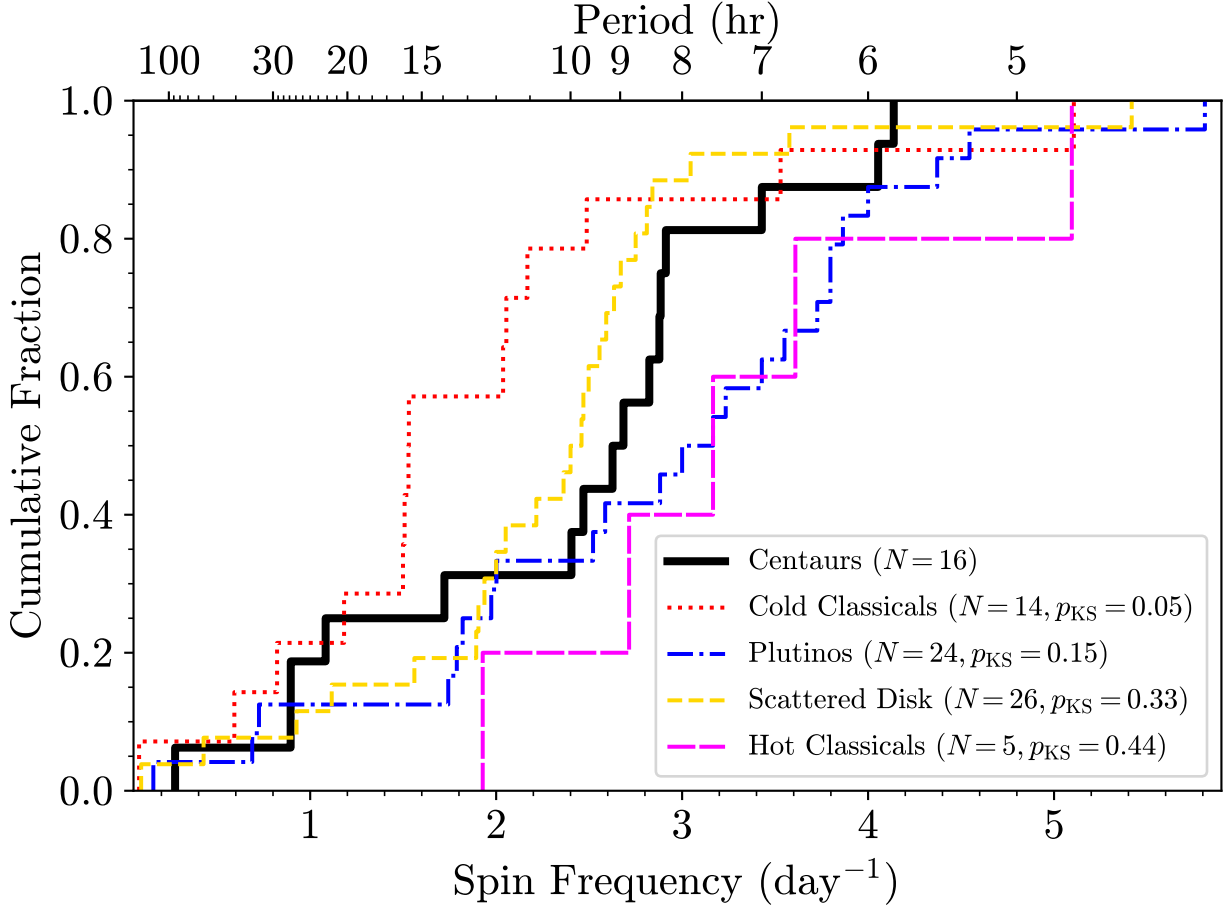


**Figure 7.** Cumulative spin rate distributions of Centaurs and other transneptunian objects. Legend indicates, for each dynamical group, sample size and the Kolmogorov-Smirnov test  $p$ -value that the sample and the Centaurs have the same spin rate distribution.

median spin period of  $\sim 14$  hr. Larger Centaurs spin faster than 2.5 rotations per day, with a median period of  $\sim 7$  hr. The three largest Centaurs are also the fastest rotators, with  $P < 7$  hr.

If a large proportion of the Centaurs are collisional fragments (see section 5.2), then collisional evolution prior to leaving the source region must have played a role in setting rotations (see section 3.9). However, energy equipartition would predict smaller Centaurs to spin faster, which argues against the observed distribution of spin frequencies being driven by collisional evolution. It may be that the smaller Centaurs hit a spin barrier at three rotations per day, which would suggest that they are gravitationally reaccumulated outcomes of collisions. If so, then the larger Centaurs were never disrupted by collisions, and retain their original spin rates.

Another possible explanation for smaller Centaurs display slower spins has to do with torques due to activity. If spin-up and spin-down are equally likely, this tends to increase the median spin period as spun-up Centaurs may be rotationally disrupted leaving a population of survivors biased towards slower rotators. This effect, investigated in D. Jewitt (2021) for Jupiter-family comets (JFCs), is a function of size, with small objects more affected than larger ones: a factor of 10 increase in size corresponds to a factor 100 increase in spin-up/down timescale (see also N. H. Samarasinha & B. E. A. Mueller 2013; J. K. Steckloff & N. H. Samarasinha 2018; T. K. Safrid et al. 2021).

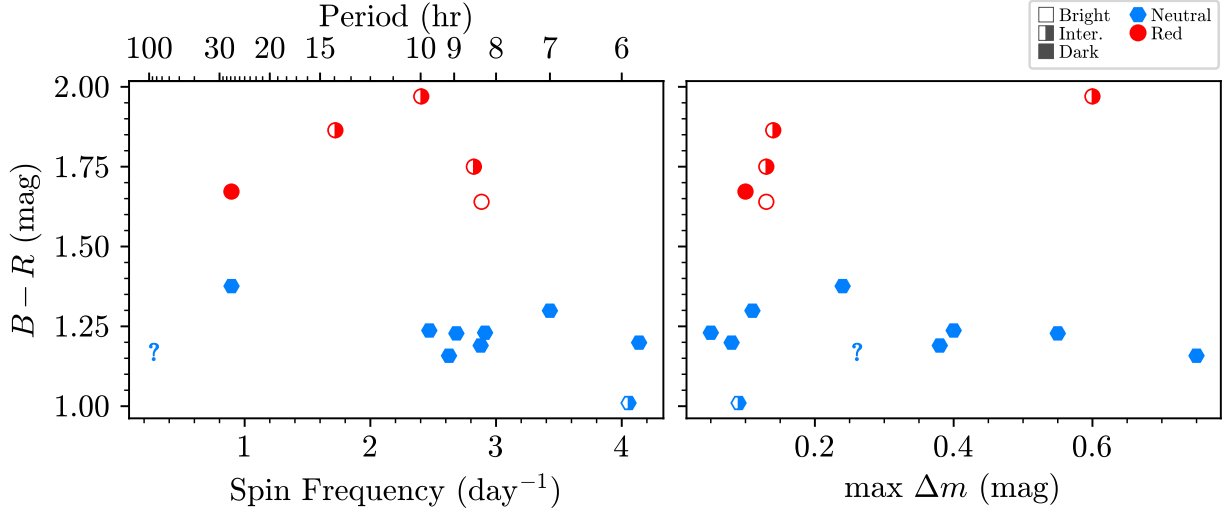


**Figure 8.** Spin frequency (left panel) and maximum  $\Delta m$  (right panel) versus  $B - R$  color. Point color and shape highlight the bimodality and the fill pattern indicates surface albedo (filled symbols for “Dark” albedos from 0.04 to 0.07; half-filled symbols for “Intermediate” albedos from 0.12 to 0.16; open symbols for “Bright” albedo 0.24; question mark indicates unknown albedo).

It is unlikely that activity can explain the presence of slower rotators and absence of faster rotators among smaller Centaurs relative to the spin rates of larger Centaurs. According to Fig. 1 in [D. Jewitt \(2021\)](#), notional Centaur-sized nuclei ( $D \sim 100$  km) should have spin-up timescales  $\sim 10^5$  yrs, comparable to the dynamical lifetimes of Centaurs. However, it is important to note that the Figure applies to JFCs with  $q \sim 1$  to 2 au and hence larger mass-loss rates. An interesting complication is that some of the Centaurs may have dipped into temporary low- $q$  orbits () where activity could have played a more important role (Chapters 7 and 3; [R. Kokotanekova et al. 2025](#); [R. P. Di Sisto et al. 2025](#)). More work is needed to understand the effect of orbital evolution and activity on Centaurs spins.

### 3.5. Shapes

A simple way to translate lightcurve variability into a shape model is to assume that it is caused by a triaxial ellipsoid object rotating around its shortest principal axis. The caveat here is that in reality many objects are not ellipsoidal but have more complex shapes (e.g., [S. A. Stern et al. 2019](#); [M. W. Buie et al. 2018](#)) making lightcurve interpretation more difficult. Multiple lightcurves obtained at several orbital longitudes can help with this ([M. Kaasalainen & J. Torppa 2001](#)), but that can be a lengthy proposition for a study of Centaurs. Nonetheless, we can continue with the simplifying assumption, and the ellipsoid minimum and maximum sky-projected cross section areas are given by

$$C_{\min} = \pi b (a^2 \cos^2 \theta + c^2 \sin^2 \theta)^{1/2} \quad (1)$$

and

$$C_{\max} = \pi a (b^2 \cos^2 \theta + c^2 \sin^2 \theta)^{1/2}, \quad (2)$$

where  $a \geq b \geq c$  are the semi-axes of the ellipsoid, and  $0 \leq \theta \leq \pi/2$  is the aspect angle, measured between the line of sight and the spin pole direction.

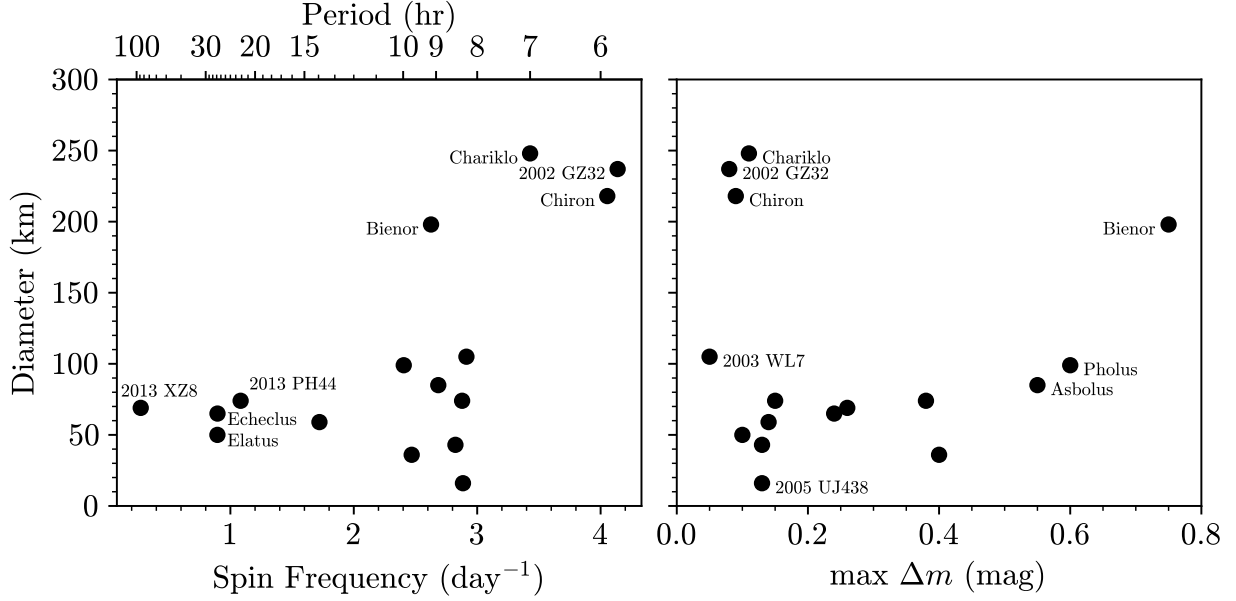


**Figure 9.** Centaur diameter plotted against spin rate (left panel) and maximum lightcurve range (right panel).

The photometric range,  $\Delta m$ , is related to ratio of those areas and given by

$$\Delta m = -2.5 \log \frac{C_{\min}}{C_{\max}} = -1.25 \log \left( \frac{\cos^2 \theta + (c/a)^2 \sin^2 \theta}{\cos^2 \theta + (c/b)^2 \sin^2 \theta} \right), \quad (3)$$

which depends only on the ellipsoid axis ratios and the aspect angle. If the ellipsoid is observed equator-on ( $\theta = \pi/2$ ), the axis ratio can be obtained directly from

$$b/a = 10^{-0.4\Delta m} \quad (4)$$

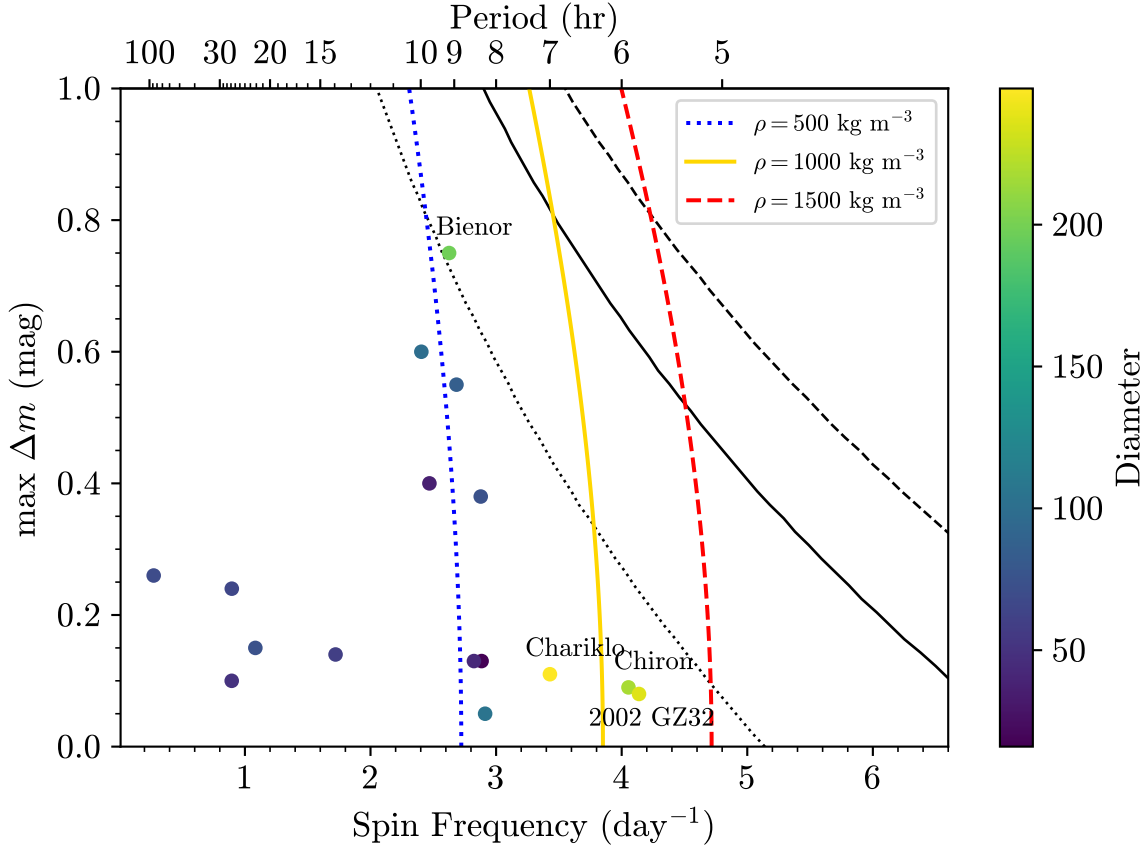
The pole orientation is generally unknown, so an observed  $\Delta m$  sets an upper limit on  $b/a$ .

Figure 9 (right panel) shows maximum lightcurve variability,  $\Delta m_{\max}$ , plotted against Centaur size. The larger Centaurs ( $D > 150$  km) display very “flat” lightcurves ( $\Delta m \lesssim 0.1$  mag), indicative of more spherical shapes. Bienor is an interesting outlier: with  $D \approx 200$  km it has the largest observed variability  $\Delta m \sim 0.75$  mag, which implies an axis ratio  $\sim 1:2$ .

The icy moons of the giant planets larger than  $D = 400$  km tend to be spherical (C. H. Lineweaver & M. Norman 2010), suggesting a transition to a regime where gravitational pull takes over material strength and causes a body to become spherical. The data on Centaurs are sparse, but indicate a transition at smaller sizes, around  $D = 100$  km. If confirmed, this difference in size at which the gravity becomes dominant should imply different bulk composition and/or internal structures between the two populations.

### 3.6. Constraints on density

A useful family of triaxial shapes to consider are the Jacobi ellipsoids. These are the hydrostatic equilibrium shapes of self-gravitating, fluid bodies of uniform density spinning with constant angular frequency (S. Chandrasekhar 1969). The shape (axis ratios) is set by each combination of spin



**Figure 10.** Lightcurve variability versus spin rate. Points shaded according to their diameter in km. Three colored lines correspond to Jacobi triaxial ellipsoids with densities 500 (dotted), 1000 (solid) and 1500  $\text{kg m}^{-3}$  (dashed), viewed equator-on. Three, more slanted and thinner, black lines indicate the minimum density that balances centripetal and gravitational acceleration at the tips of prolate ellipsoids (dotted, solid and dashed correspond to the same densities as for the colored lines.)

frequency and density, so the latter can be estimated from the lightcurve information, subject to the hydrostatic fluid behaviour assumption.

Figure 10 plots lines of  $\Delta m$  against spin frequency for Jacobi ellipsoids of different densities seen equator-on. Centaur lightcurve properties are overplotted and shaded according to each body’s size. If Centaurs are in hydrostatic equilibrium, none spins fast enough to require bulk densities much larger than  $1000 \text{ kg m}^{-3}$ . Larger Centaurs ( $D \gtrsim 200 \text{ km}$ ) concentrate near the density upper limit, mainly due to their fast spins. Smaller Centaurs spin slowly and only require densities of a few hundred  $\text{kg m}^{-3}$  to sustain their shapes. We note, however, that occultation measurements of Chariklo and its rings have revealed a shape that is not well matched by a figure of hydrostatic equilibrium (B. E. Morgado et al. 2021). If we simply balance centrifugal and gravitational accelerations at the tip of prolate ellipsoids to obtain a minimum bulk density, then all Centaurs spin below the critical rate for a bulk density of  $500 \text{ kg m}^{-3}$  (see black, slanted lines in Fig. 10) which is suggestive of a spin barrier (see section 3.9).



### 3.7. Binaries, contact binaries and rings

Two known binaries, (42355) Typhon and Echidna and (65489) Ceto and Phorcys, traverse the Centaur region. They were resolved in HST observations (K. S. Noll et al. 2006; W. M. Grundy et al. 2007) with apparent separations 0.1 to 0.2 arcsec ( $1330 \pm 130$  and  $1840 \pm 48$  km, respectively). However, both have orbits extending far beyond Neptune<sup>8</sup> and are thus excluded from this review. None of the Centaurs in Table 1 is a resolved, wide binary (Chapter 9; A. Sickafoose et al. 2025).

Neither do the Centaur rotational properties suggest strong contact binary candidates, which are usually inferred from large lightcurve variability,  $\Delta m > 0.9$  mag (S. S. Sheppard & D. Jewitt 2004; O. Gnat & R. Sari 2010; P. Lacerda et al. 2014a; A. Thirouin & S. S. Sheppard 2018). Bilobed shapes can produce similarly large variation (P. Descamps 2016). Contact binaries seem abundant in many small body populations (S. S. Sheppard & D. Jewitt 2004; R. K. Mann et al. 2007; P. Lacerda 2011; A. McNeill et al. 2018; A. Thirouin & S. S. Sheppard 2018; M. R. Showalter et al. 2021). Even though none of the Centaurs in Table 1 displays such extreme variability, Bienor’s  $\Delta m = 0.75$  mag can in principle be caused by an eclipsing binary of two equal spheres. Recent work suggests the contact binary/bilobed shapes observed in JFCs visited by spacecraft can originate in the Centaur region via spin-up due to sublimation torques (T. K. Safrid et al. 2021). KBO Arrokoth is evidence that such shape can already exist in the Kuiper Belt. We note that unambiguous shape determination for these objects requires complementary observations. From the ground, dense, multi-chord occultation data may help solve the ambiguity, but only spacecraft flybys can provide ground truth.

A number of factors could contribute to attenuate a lightcurve’s range. For instance, the presence of an unknown secondary in unresolved observations from the ground can complicate the interpretation of the lightcurve. The additional cross section, if present, dampens the lightcurve variation giving the impression of a less elongated primary object. Rings such as Chariklo’s (F. Braga-Ribas et al. 2014), and possibly Chiron’s (J. L. Ortiz et al. 2015; J. D. Ruprecht et al. 2015; A. Sickafoose et al. 2025), and debris or dust in the coma of active Centaurs also contribute additional cross section in unresolved lightcurve observation (Chapter 9; A. Sickafoose et al. 2025). The result is a lower, contaminated lightcurve  $\Delta m_c$ , given by

$$\Delta m_c = -2.5 \log \left( \frac{C_{\min} + C_{\text{coma}}}{C_{\max} + C_{\text{coma}}} \right) = -2.5 \log \left( \frac{k + (b/a)}{k + 1} \right) \quad (5)$$

where  $k = C_{\text{coma}}/C_{\max}$  is the rings/coma cross section relative to the maximum nucleus cross section (J. X. Luu & D. C. Jewitt 1990). Observations of active Centaurs (J. X. Luu & D. C. Jewitt 1990; D. Jewitt 2009) and Chariklo’s ring (F. Braga-Ribas et al. 2014) show that  $k < 0.5$  for the objects in Table 1. We note that the level of activity (and  $k$ ) varies with time, so they are relevant if occurring at the time the lightcurve is measured. For example, if Chiron’s cross-section would include a contemporaneous  $k = 0.5$  contribution from activity, debris, rings, or a small unresolved companion, then its undiluted lightcurve would vary by  $\Delta m = 0.14$  mag, compared to the apparent  $\Delta m = 0.09$  mag. For Bienor, the most photometrically variable Centaur, a relative contribution of  $k = 0.25$  would imply an undiluted  $\Delta m = 1.1$  mag. Attempts to detect activity for this Centaur have only rendered an upper limit  $k < 0.001$  (D. Jewitt 2009; M. M. Dobson et al. 2023), but rings or an unresolved companion cannot be ruled out. Finally, significant obliquity of the spin pole, combined

<sup>8</sup>  $Q_{T\&E} = 57.6$  au,  $Q_{C\&P} = 181.1$  au

with an observing geometry away from equinox (equator-on), would also “hide” an elongated shape (see Eq. 3).

### 3.8. Spin vectors and obliquities

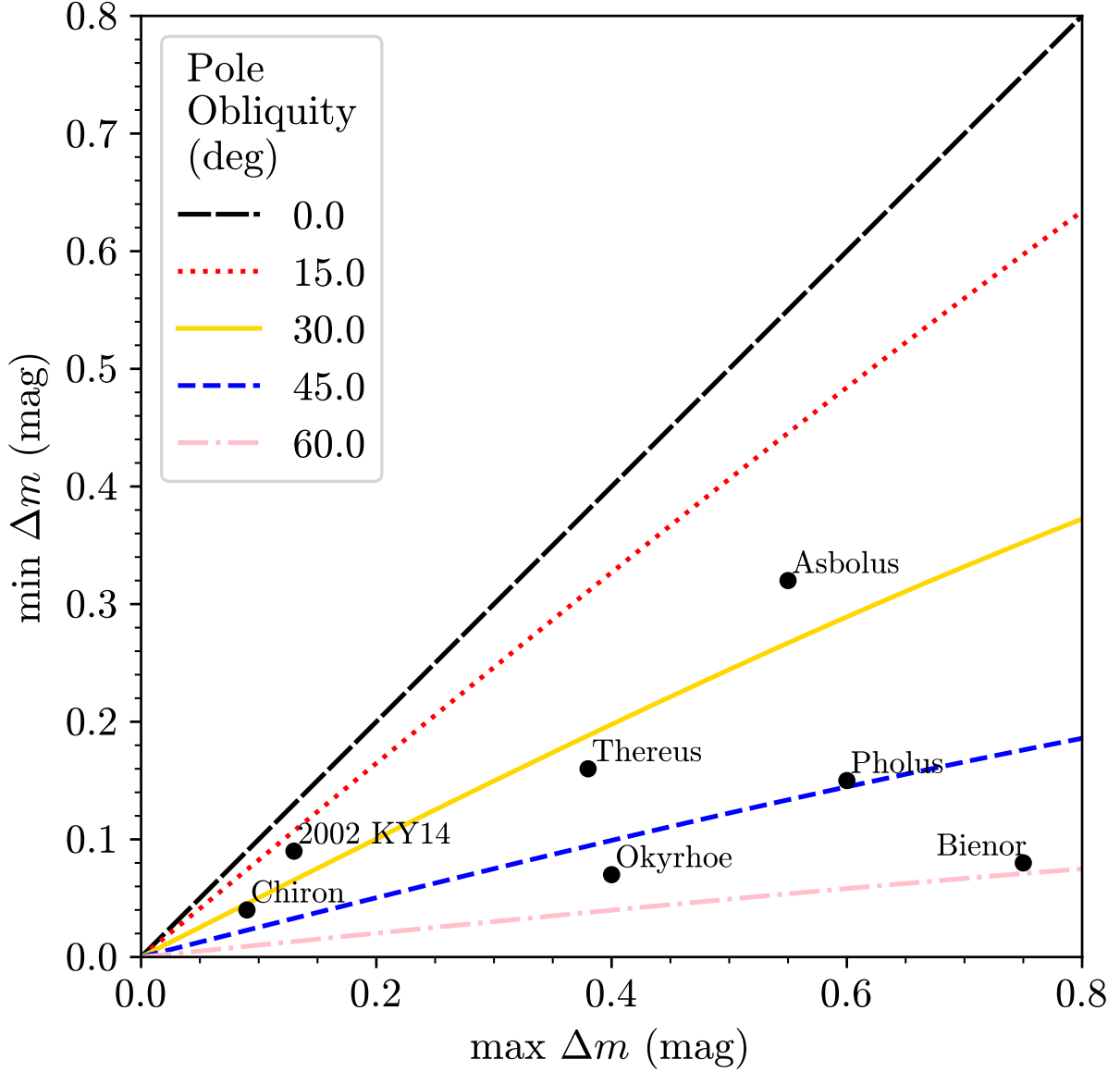
Lightcurve measurements at different aspect angles (the angle between the line of sight and the spin pole) are needed to constrain the spin pole orientation. Such studies of the changing lightcurves of Pholus and Bienor over 13 and 16 years, respectively, have yielded spin poles directed towards ecliptic latitude  $\beta = +30 \pm 5$  deg and longitude  $\lambda = 145 \pm 5$  deg for Pholus, and  $\beta = 50 \pm 3$  deg and longitude  $\lambda = +35 \pm 8$  deg for Bienor (S. C. Tegler et al. 2005; E. Fernández-Valenzuela et al. 2017). Reliable pole solutions are challenging (reliable lightcurves are needed spanning a wide range of ecliptic longitudes) and hence still rare: Pholus and Bienor are the only cases. For distant objects of moderate inclination, two measurements of  $\Delta m$  taken sufficiently far apart along the orbit of an object can set limits on its obliquity,  $\varepsilon$ , which is the angle between the pole and the normal to the orbit plane (P. Lacerda 2011). At  $\varepsilon = 90$  deg there is a big variation in  $\Delta m$  (from a maximum value when seen equator-on down to 0 at pole-on geometry), while for  $\varepsilon = 0$  there is none.

Figure 11 plots lines of minimum vs maximum  $\Delta m$  for Jacobi ellipsoids of different obliquities. A given shape ( $b/a$ ) implies a maximum  $\Delta m = -2.5 \log(b/a)$  and the obliquity defines what the minimum  $\Delta m$  will be according to Equation 3, where the minimum possible aspect angle is  $\theta = 90 - \varepsilon$  in degrees. Overplotted are the Centaurs with measured minimum and maximum lightcurve ranges, which are respectively upper and lower limits to the real min  $\Delta m$  and max  $\Delta m$ . Under the figure’s idealized shape assumptions, the lines indicate minimum obliquity for each Centaur. Pholus’s pole obliquity, calculated between the pole solution and the normal to its orbit plane (inclination  $i = 24.7$  deg and longitude of ascending node  $\Omega = 119.4$  deg) is  $\varepsilon \approx 73$  deg. For Bienor ( $i = 20.7$  deg and  $\Omega = 337.7$  deg) the pole solution implies an obliquity  $\varepsilon \approx 58$  deg. These do not contradict Fig. 11’s minimum obliquities of  $\varepsilon_{\min} \sim 45$  deg for Pholus and  $\varepsilon_{\min} \sim 60$  deg for Bienor. The figure suggests that Centaurs have considerable obliquities. Except Asbolus and 2002 KY14, the remaining 5 Centaurs have obliquities in excess of 30 deg, and three have obliquities larger than 45 deg, if their axes ratios are approximately Jacobi-ellipsoidal. Significant obliquity can cause interesting surface illumination and heating patterns, which are important for understanding Centaur activity (see, e.g., Chapters 7 and 8; R. Kokotanekova et al. 2025; J. Bauer et al. 2025).

### 3.9. Processes affecting rotation

As mentioned above, a number of processes can affect the rotational properties of Centaurs. Collisions, discussed in detail in section 5.2, will most likely lead to spin-up, which for the smaller objects can lead to rotational breakup (P. Lacerda 2005). Collisions are unlikely in the Centaur phase, so spins imposed by this process should have been set before the objects left their reservoir in the transneptunian disk.

Torques from cometary activity can cause both spin up or spin down, with equal probability. Such sublimation torques are likely negligible at Centaur distances and certainly for the larger objects, but a scenario in need of more careful study are those objects that have dipped closer to the sun during their dynamical evolution (see, e.g., 39P/Oterma and P/2019 LD2 discussed in Chapter 3; R. P. Di Sisto et al. 2025). Sublimative torques may play a role in those cases.



**Figure 11.** Maximum vs minimum lightcurve variability of Centaurs. Lines correspond to Jacobi ellipsoids spinning around the minor principal axis seen equator-on ( $\max \Delta m$ ) and at minimum aspect angle along the orbit ( $\min \Delta m$ ).

Processes that lead to the formation of binaries or rings, and their dynamical evolution may also set or affect rotation. This remains largely unexplored for Centaurs, mostly because of the lack of data to constrain any proposed models.

These processes would manifest in the observations in different ways. Collisions cause net spin-up and eventually lead to rotational breakup, setting a spin-barrier and a lower limit to the size of the survivors. Figure 10 hints at a rotational limit even though the data are still sparse. A simple collisional evolution model in an assumed massive, primordial Kuiper Belt would result in a minimum size of survivors of a few tens of km in radius (P. Lacerda 2005). Centaurs and descendant JFCs an order of magnitude smaller are observed, but the model is too rudimentary to allow conclusions to

be drawn. Sublimative torques lead to a random walk in spin rate, causing the survivor spin rate distribution to be skewed towards slow rotators while also imposing a maximum spin barrier.

#### 4. LIMITATIONS OF MEASUREMENT METHODS

Many observational techniques to derive physical properties suffer from limitations. This does not mean that the techniques are not useful, only that one must interpret results carefully. We describe some of the particulars here. Many of these issues are of course common to all small-bodies, not just to Centaurs.

As was mentioned earlier, visible-wavelength photometry of a bare (inactive) Centaur can eventually yield an absolute magnitude  $H$  but requires an albedo in order to find the diameter. More specifically, the well-known relationship (see [P. Pravec & A. W. Harris 2007](#)) is

$$D_{km} = \frac{2a_{km}10^{0.2m_{\odot\lambda}}}{\sqrt{p_{\lambda}}}10^{-0.2H_{\lambda}}, \quad (6)$$

where  $D_{km}$  is the diameter in km,  $a_{km}$  is a constant, the number of km in 1 au, subscript  $\lambda$  indicates a quantity at a specific wavelength,  $m_{\odot}$  is the monochromatic magnitude of the Sun and  $p$  is the geometric albedo. Thus we see that this conversion in fact requires additional information such as the geometric albedo ( $p$ ), and the phase darkening law and rotational context (for a better  $H$ ). Extensive photometry on rotational and seasonal timescales can eventually resolve some of this problem.

But even overcoming all of these issues, there is still a problem of what does it mean to have a diameter of a non-spherical object (see Section 3). With visible photometry, this is often effectively the geometric-mean of the cross-section axes, but this isn't necessarily the best answer. If the ultimate goal is, say, to understand the mass distribution of Centaurs, then one could argue that the 'best' diameter to use is one that is the geometric mean of the three ellipsoid axes,  $\sqrt[3]{abc}$ . In a typical scenario, if one measures the object's light curve, assumes an equator-on view, and assumes that  $b = c$ , then one's calculation of the volume-derived radius – i.e.,  $a(b/a)^{2/3}$  – is off by a factor of  $\sqrt[3]{c/b}$  from the true answer. If every nucleus had the same  $c/b$  axial ratio, then this would just mean that the size distribution would as a whole be shifted sideways. Of course it is likely the case that  $c/b$  is not constant across objects, and so there could be a slope bias in the size distribution. This would be especially deleterious if the largest objects in the size distribution have  $c/b$  values significantly below unity; usually the largest objects in a size distribution are few in number, and if they are widely incorrect, it can significantly affect the resulting power-law exponent.

To return to the problem of determining the size, certainly infrared techniques, using measurements of the thermal radiation, have given us great improvements. Since the square of the diameter is, broadly speaking, proportional to the thermal infrared flux density divided by  $(1 - pq_{ph})$ , where  $q_{ph}$  is the phase integral, and since  $pq_{ph}$  is generally small, the systematic uncertainty is in principle lower. Nonetheless, the rotational context can still be a problem, and the phase darkening of thermal emission is not well understood. The temperature map of a Centaur's surface may not be well known, either because the object's shape is poorly constrained or because the fundamental thermal quantities (thermal inertia, thermal diffusivity) are not well constrained, or both. Detailed work on the thermal properties of near-Earth asteroids (e.g., [E. L. Wright 2007](#); [E. Wright et al. 2018](#); [E. S. Howell et al. 2018](#); [M. Mommert et al. 2018](#); [S. A. Myers et al. 2023](#)) reveals the simplistic thermal models to interpret single-snapshot thermal-IR photometry of highly nonspherical objects can give diameters that are significantly off. Such a problem can be even more severe for distant objects like Centaurs

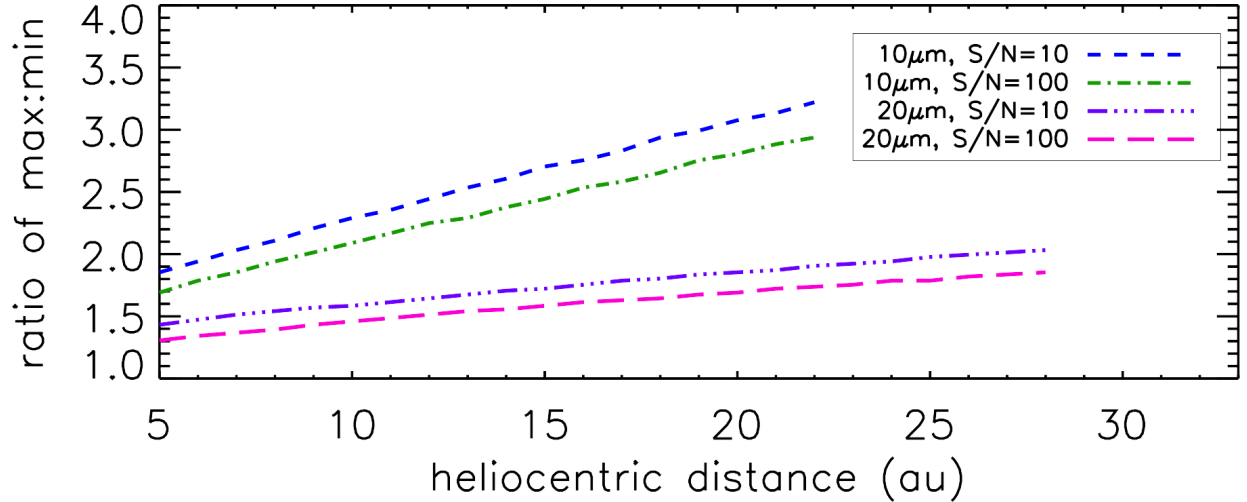


**Figure 12.** Example of the problem with single-band photometry of the thermal-IR emission from a Centaur. The plot shows how one-band mid-IR photometry of a Centaur at a given heliocentric distance results in a large uncertainty in the diameter. The  $y$ -axis shows the ratio of the maximum and minimum possible diameters. In this case, we assumed a geometric albedo of 0.08, emissivity of 0.95, and a phase angle of  $2^\circ$ . We used NEATM (A. W. Harris 1998), and assumed a beaming parameter range of 0.8 to 1.3. We tried two wavelengths (10 and 20  $\mu\text{m}$ ) and two photometric  $S/N$  values (100 and 10). The 10  $\mu\text{m}$  lines stop at 22 au since past that, that wavelength is dominated by reflected sunlight. The 20  $\mu\text{m}$  lines stop at 28 au since a phase angle of 2 degrees is impossible past that. For more distant (and thus cooler) Centaurs, the range of possible diameters spans a large factor. This uncertainty ignores the applicability of NEATM in the first place, since more distant objects are more likely to be fast rotators.

where photometry in the vicinity of 10  $\mu\text{m}$  lies on the Wien-law side of a thermal continuum. This is demonstrated for a particular case in Figure 12, where there is just one band of mid-IR photometry and so NEATM and a beaming parameter range is assumed. For example, suppose we have thermal-IR photometry at a wavelength of 10 microns that has yielded a  $S/N = 10$  measurement of an object that is 10 au from the Sun. Assuming that the beaming parameter is between 0.8 and 1.3, we find from the plot that a wide range of radii fit the data point, with the maximum possible radius being  $\mathcal{R} = 2.3$  times larger than the minimum. This corresponds to a fractional uncertainty in the radius of  $(\mathcal{R} - 1)/(\mathcal{R} + 1) = 39\%$ , quite significant. The figure shows that the result has some dependence on  $S/N$ , since less accurate photometry will let more possible values of NEATM parameters work, but this problem persists even for high quality photometry ( $S/N = 100$  in the plot). In any case, this demonstrates that multiband photometry improves the ability to apply more sophisticated thermal models.

As discussed in Eq. 5, a Centaur’s coma will complicate finding a Centaur’s physical properties. In principle an extraction technique can be done (P. L. Lamy & I. Toth 1995; C. M. Lisse et al. 1999; M.-T. Hui & J.-Y. Li 2018) but the method loses reliability the coarser the spatial resolution of the imaging and the more dominant the coma’s flux is against the nucleus’s. While traditionally one of the criteria for determining if an object has cometary activity is to look for extended emission beyond the PSF ((see, e.g., D. Jewitt 1991), it is possible for comets to be active and yet hide coma within the PSF, as is the case apparently for ecliptic-comet 2P/Encke (Y. R. Fernández et al. 2005).

For more distant objects such as Centaurs, it would be even easier to be fooled into thinking that an ostensibly PSF-looking Centaur is bare when it in fact has some cometary activity.

We mention one further limitation here: the spatial resolution limitation for identifying a Centaur as a binary (cf. §3.7). HST has been used to show that at least about one-fifth of cold classical TNOs are binaries (K. S. Noll et al. 2008; S. B. Porter et al. 2024), with the limitation there for detection being that the secondary needs to be bright enough and at least several hundred kilometers from the primary. Searches that use HST to look for binarity among Centaurs include, e.g., that of J. Li et al. (2020), who looked at 23 objects that would be included in our Centaur definition here (among many other objects) but found no binaries, even though their linear spatial resolution was roughly about twice as good as it is for cold-classical TNOs. In any case, if there is a population of ‘tight’ Centaur binaries, it may be necessary to conduct a search where spatial resolutions better than  $\sim 100$  km are possible. This is 14 milliarcsec for an object 10 au away, i.e. just under 0.5 JWST NIRCам short-wavelength pixels. It would certainly be interesting to determine definitively whether the binary fraction of the Centaurs were much lower than that of the TNO population.

## 5. COMPARATIVE PLANETOLOGY OF OUTER SOLAR SYSTEM BODIES

The term “comparative planetology” evokes an approach of taking a set of diverse measurements and properties of individual objects in search of a deeper understanding of the set. Much of what we call comparative planetology has been driven by comparing and contrasting terrestrial planets, giant planets, dwarf planets where individual properties matter a great deal. When applying this notion to small bodies, a different framework and approach becomes important.

For small bodies, individual properties are still important but the distribution of those properties across the full population provide far more insight. A fantastic example of this approach is the data from the Sloan Digital Sky Survey (SDSS) (Ž. Ivezić et al. 2001, 2002). A prominent example of this work is showing the compositional ties within and between asteroid collisional families. While we do not yet have a dataset comparable to SDSS that covers the entire Solar System, we do expect such fundamental data to come from future surveys. In the meantime, we make do with such data as we have. The critical point here is to focus on the properties of populations of small bodies and look for insight in comparing and contrasting populations. For this section, comparative planetology will refer to the comparison of population properties and what it can tell us.

### 5.1. *Centaur Shapes*

The concept of a “primordial” object is unfortunately an overused and poorly codified term used widely in planetary science. At one time or another the term primordial has probably been applied to every small body in the Solar System.

With the successful flyby of Arrokoth by New Horizons, we finally have an object truly worthy of the term. As discussed by W. B. McKinnon et al. (2020), Arrokoth is now helping to more clearly define the concept of what a primordial object is. Here we have an example of an object that has remained essentially untouched since the end of the accretion phase of building our Solar System (or at least since the time of thermal equilibration once the disk cleared). As such, it directly informs and constrains theories of how the accretion process works. As a cold-classical Kuiper Belt object (CCKBO), we can look upon these objects as being truly primordial. It would appear that every other population of small body, while made up of primordial material, has been more affected by post-accretional processes than what we understand for CCKBOs.



An important question to address is the extent and nature of any processing that has been at work on Centaurs. Quantifying the amount of processing will go far in placing them in context within the other populations of small bodies and help identify the source population and pathway by which an object becomes a Centaur.

Our best prospect, short of spacecraft missions, for assessing the primordial nature of Centaurs lies with detailed stellar occultation observations. Observations of Jupiter Trojans conducted in support of the Lucy mission show that all the targets have significantly more complicated shapes than exhibited by Arrokoth (e.g., [M. W. Buie et al. 2021](#); [S. Mottola et al. 2023, 2024](#)). In this case, this constraint is not about the contact binary shape of Arrokoth. None of the Lucy targets is an obvious contact binary though we cannot exclude some being badly distorted contact binaries. The more interesting constraint is that the Lucy targets do not have smooth (i.e., elliptical) shapes and all show significant modification with respect to Arrokoth. This result runs over the range of 30-120 km for the Lucy targets. It remains to be seen if there are any remaining signatures of the primordial shape for these objects and the definitive answers will come with the culmination of that mission.

There are three key observables in the shape of a small body that are likely to be important clues tracing back to primordial shape and thus the degree of processing that Centaurs have undergone: (1) a contact binary shape that is consistent with a gentle merger (though see [T. K. Safrit et al. 2021](#)), (2) highly oblate shape, and (3) a smooth shape. There may be other signatures we do not yet know enough about, such as the frequency of tight binaries, since we do not have good knowledge of this for any other distant population.

## 5.2. *Collisions*

Collisions can significantly alter small body populations. This is particularly evident in the main asteroid belt. Its size distribution shows clear signs of being sculpted by collisions ([W. F. Bottke et al. 2005, 2020](#)). Furthermore, the main asteroid belt contains many collisional families, which can be traced back to catastrophic disruptions of larger bodies (e.g., [D. Vokrouhlický et al. 2010](#); [J. Licandro et al. 2012](#); [F. Spoto et al. 2015](#); [B. T. Bolin et al. 2017](#)). In contrast, the Jupiter Trojans have only one major collisional family, the one of Eurybates ([M. Brož & J. Rozehnal 2011](#); [R. Marschall et al. 2022](#)).

The amount of collisional evolution is driven by the dynamical evolution of a small body population. There is now a general consensus that planetesimals that end up as Centaurs and JFCs formed in an original reservoir, the primordial Kuiper belt (PKB), located between 20-40 au from the Sun (e.g., [D. Nesvorný 2018](#)). From there, they were scattered into the current trans-Neptunian region. From that region, the scattered disk in particular acts as the source reservoir for Centaurs and JFCs (e.g., [M. J. Duncan & H. F. Levison 1997](#)). Crucially, the scattering phase of planetesimals must occur as the gas disk dissipates to prevent the damping of the scattered orbits. This is well described by the final phase of planetesimal-driven migration, particularly Neptune’s migration (e.g., [D. Nesvorný et al. 2018](#); [D. Nesvorný 2021](#)).

The collisional environment of a Centaur can thus be divided into three phases: 1) the period in the PKB and subsequent scattering into the current trans-Neptunian region; 2) the period in the scattered disk; 3) the Centaur phase ([W. F. Bottke et al. 2023](#)). Phase 1 in the PKB may only last a few tens of millions of years. Nevertheless, it is the phase with the largest number of impacts because of the large mass of the PKB (several tens of Earth masses) compared to the scattered disk (1/400 of the initial PKB; [W. F. Bottke et al. 2020](#); [D. Nesvorný et al. 2020](#)). Phase 2 lasts for most

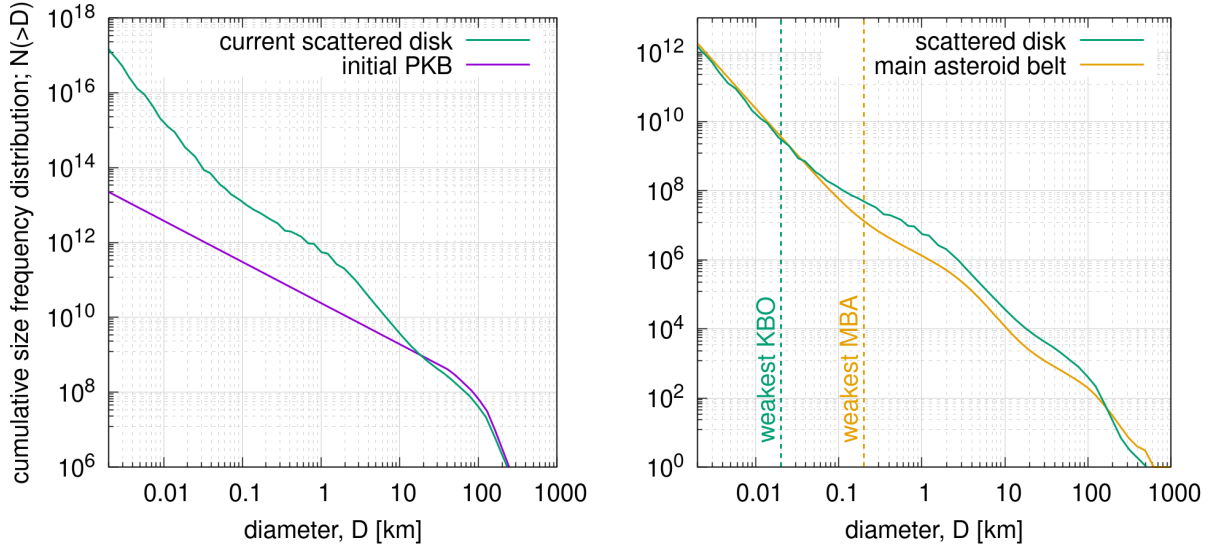


**Figure 13.** The left panel shows the cumulative size frequency distribution (CSFD) of the initial primordial Kuiper-belt (PKB) and the collisionally evolved CSFD of the current day scattered disk according to [W. F. Bottke et al. \(2023\)](#). The dynamical depletion of the current scattered disk is not shown. The right panel shows the CSFD of the current day scattered disk ([W. F. Bottke et al. 2023](#)) and the main asteroid belt ([W. F. Bottke et al. 2020](#)). The dashed lines show the approximate location of the weakest Kuiper-belt object (KBO) and main belt asteroid (MBA). The scattered disk SFD has been scaled to be on the same order of magnitude of the main belt.

of the lifetime of the Solar System (4.5 Gyr) and may still contribute moderately to the collisional evolution. The final phase, when objects are scattered into the giant planet region, lasts only a few million years and will not contribute in any notable way to the collisional evolution of Centaurs. In this phase, sublimation-driven activity will dominate any collisional evolution (see, e.g., Chapters 5, 7, and 8; [N. Peixinho et al. 2025](#); [R. Kokotanekova et al. 2025](#); [J. Bauer et al. 2025](#)).

Another crucial ingredient to understanding collisional evolution is the initial size distribution. Current planetesimal formation models suggest that planetesimals form via the streaming instability. This disk instability accumulates dust particles in clouds massive enough for self-gravity to cause the cloud to collapse and directly form large planetesimals. This mechanism predicts an initial Gaussian size distribution centred around  $D = 100$  km (e.g., [J. B. Simon et al. 2016](#); [U. Schäfer et al. 2017](#); [H. Klahr & A. Schreiber 2020](#)). While these are models, the current Kuiper belt has a distinct bump around 100 km. This is in line with a leftover streaming instability size distribution.

[W. F. Bottke et al. \(2023\)](#) showed that an initial streaming instability size distribution can indeed evolve into the current scattered disk size distribution. They showed that this evolution is consistent with (i) crater SFDs on icy satellites and KBOs (e.g., [K. N. Singer et al. 2019](#); [K. Zahnle et al. 2003](#); [P. M. Schenk et al. 2004](#); [M. R. Kirchoff & P. Schenk 2010](#)), and (ii) observed SFDs of populations derived from the PKB (e.g., Jupiter’s Trojans) ([I. Wong & M. E. Brown 2015](#); [F. Yoshida & T. Terai 2017](#)). The craters on icy satellites were used to infer the size distribution of the PKB population scattered onto planet-crossing orbits and those that went to the scattered disk. Figure 13 shows the initial and evolved Kuiper belt size distribution. It exhibits a wavy shape characteristic of collisional evolution.

The Kuiper belt thus appears to be similarly collisionally evolved as the main asteroid belt with one significant difference (Fig. 13). While the weakest body in the asteroid belt has a diameter of roughly 200 m, it is only 20 m in the scattered disk (Fig. 13). This shift in the weakest bodies shifts the location of the “collisional wave” of the size distribution of asteroids to KBOs to smaller sizes.

The fact that the scattered disk size distribution can be explained by collisionally evolving a streaming instability distribution indicates that most smaller bodies in the scattered disk, and by extension the Centaur population, are collisional fragments. [R. Marschall et al. \(2023\)](#) argue that 50% of scattered disk objects/comets/centaurs larger than 10 km should be collisional fragments. For objects larger than 1 km, at least 95% of objects are fragments. In contrast, large Centaurs (100 km and larger) are, to a large extent, untouched by disruption and thus the most “pristine” in this respect.

## 6. FUTURE PROSPECTS

As with many things in astronomy, one way to address some of the issues we have described above is with large amounts of data, and especially data that sample new regimes of faintness. Number statistics are crucial. New datasets from Vera C. Rubin Observatory and NEO Surveyor promise to improve the discovery rate and characterization of many Centaurs ([A. K. Mainzer et al. 2023](#); [M. E. Schwamb et al. 2023](#); [E. Fernández-Valenzuela et al. 2025](#)). Further data from existing surveys like Pan-STARRS will continue to help us with photometric coverage. This is especially useful for objects like Centaurs that tend to have multidecade orbital periods, so it takes a while for our vantage point (i.e. sub-Earth latitude) to change significantly. Disentangling the photometric manifestations of a Centaur’s shape, rotation period, spin axis direction, color/albedo variations, and phase darkening can be challenging, just as it is with any asteroid. Add onto that the possibility that some Centaurs could have hiccups or outbursts of activity, that may or not be resolved, and it is clear that denser photometric coverage, at a range of cadences, can be necessary.

Insights into cometary activity (see Chapter 8; [J. Bauer et al. 2025](#)), especially such activity at distances from the Sun where water ice sublimation is *not* the main driver, will be useful for further studies of how Centaur surfaces change. This can include more detailed assessment of Rosetta’s observations of 67P when that comet was far from the Sun. But it may also require sending a spacecraft to study a Centaur up close (see Chapter 16; [W. Harris et al. 2025](#)). Once we can treat a Centaur as a geologic object it will surely improve our understanding of the observations of a Centaur as an astronomical object.

## ACKNOWLEDGMENTS

We thank two anonymous referees whose helpful reviews improved our manuscript.

## REFERENCES

- |   |   |
|---|---|
| <p>Bauer, J., Ivanova, O., McKay, A., &amp; Sarid, G.<br/>2025, in <i>Centaurs</i>, ed. K. Volk, M. Womack, &amp;<br/>J. Steckloff (IOP Publishing), 8–1—8–23,<br/>doi: <a href="https://doi.org/10.1088/2514-3433/ada267ch8">10.1088/2514-3433/ada267ch8</a></p> | <p>Bolin, B. T., Delbo, M., Morbidelli, A., &amp; Walsh,<br/>K. J. 2017, <i>Icarus</i>, 282, 290,<br/>doi: <a href="https://doi.org/10.1016/j.icarus.2016.09.029">10.1016/j.icarus.2016.09.029</a></p> <p>Bottke, W. F., Durda, D. D., Nesvorný, D., et al.<br/>2005, <i>Icarus</i>, 175, 111,<br/>doi: <a href="https://doi.org/10.1016/j.icarus.2004.10.026">10.1016/j.icarus.2004.10.026</a></p> |
|---|---|

- Bottke, W. F., Vokrouhlický, D., Ballouz, R. L., et al. 2020, *AJ*, 160, 14, doi: [10.3847/1538-3881/ab88d3](https://doi.org/10.3847/1538-3881/ab88d3)
- Bottke, W. F., Vokrouhlický, D., Marshall, R., et al. 2023, *PSJ*, 4, 168, doi: [10.3847/PSJ/ace7cd](https://doi.org/10.3847/PSJ/ace7cd)
- Braga-Ribas, F., Sicardy, B., Ortiz, J. L., et al. 2014, *Nature*, 508, 72, doi: [10.1038/nature13155](https://doi.org/10.1038/nature13155)
- Brož, M., & Rožehnal, J. 2011, *MNRAS*, 414, 565, doi: [10.1111/j.1365-2966.2011.18420.x](https://doi.org/10.1111/j.1365-2966.2011.18420.x)
- Buie, M. W., Zangari, A. M., Marchi, S., Levison, H. F., & Mottola, S. 2018, *AJ*, 155, 245, doi: [10.3847/1538-3881/aabd81](https://doi.org/10.3847/1538-3881/aabd81)
- Buie, M. W., Keeney, B. A., Strauss, R. H., et al. 2021, *PSJ*, 2, 202, doi: [10.3847/PSJ/ac1f9b](https://doi.org/10.3847/PSJ/ac1f9b)
- Chandrasekhar, S. 1969, *Ellipsoidal figures of equilibrium* (Yale University Press, New Haven, CT)
- Delsanti, A., Hainaut, O., Jourdeuil, E., et al. 2004, *A&A*, 417, 1145, doi: [10.1051/0004-6361:20034182](https://doi.org/10.1051/0004-6361:20034182)
- Descamps, P. 2016, *Icarus*, 265, 29, doi: [10.1016/j.icarus.2015.10.010](https://doi.org/10.1016/j.icarus.2015.10.010)
- Di Sisto, R. P., Gallardo, T., & Dones, L. 2025, in *Centaurs*, ed. K. Volk, M. Womack, & J. Steckloff (IOP Publishing), 3–1—3–28, doi: [10.1088/2514-3433/ada267ch3](https://doi.org/10.1088/2514-3433/ada267ch3)
- Dobson, M. M., Schwamb, M. E., Benecchi, S. D., et al. 2023, *PSJ*, 4, 75, doi: [10.3847/PSJ/acc463](https://doi.org/10.3847/PSJ/acc463)
- Duffard, R., Pinilla-Alonso, N., Santos-Sanz, P., et al. 2014, *A&A*, 564, A92, doi: [10.1051/0004-6361/201322377](https://doi.org/10.1051/0004-6361/201322377)
- Duncan, M., Levison, H., & Dones, L. 2004, in *Comets II*, ed. M. C. Festou, H. U. Keller, & H. A. Weaver (Univ. Arizona Press, Tucson, AZ), 193
- Duncan, M. J., & Levison, H. F. 1997, *Science*, 276, 1670, doi: [10.1126/science.276.5319.1670](https://doi.org/10.1126/science.276.5319.1670)
- Fernández, Y. R., Lowry, S. C., Weissman, P. R., et al. 2005, *Icarus*, 175, 194, doi: [10.1016/j.icarus.2004.10.019](https://doi.org/10.1016/j.icarus.2004.10.019)
- Fernández-Valenzuela, E., Guilbert-Lepoutre, A., Schwamb, M. E., et al. 2025, in *Centaurs*, ed. K. Volk, M. Womack, & J. Steckloff (IOP Publishing), 14–1—14–16, doi: [10.1088/2514-3433/ada267ch14](https://doi.org/10.1088/2514-3433/ada267ch14)
- Fernández-Valenzuela, E., Ortiz, J. L., Duffard, R., Morales, N., & Santos-Sanz, P. 2017, *MNRAS*, 466, 4147, doi: [10.1093/mnras/stw3264](https://doi.org/10.1093/mnras/stw3264)
- Fornasier, S., Lellouch, E., Müller, T., et al. 2013, *A&A*, 555, A15, doi: [10.1051/0004-6361/201321329](https://doi.org/10.1051/0004-6361/201321329)
- Fraser, W. C., Dones, L., Volk, K., Womack, M., & Nesvorný, D. 2024, in *Comets III*, ed. K. J. Meech, M. R. Combi, D. Bockelée-Morvan, S. N. Raymond, & M. E. Zolensky (Univ. Arizona Press, Tucson, AZ), 121–152
- Gnat, O., & Sari, R. 2010, *ApJ*, 719, 1602, doi: [10.1088/0004-637X/719/2/1602](https://doi.org/10.1088/0004-637X/719/2/1602)
- Grundy, W. M., Stansberry, J. A., Noll, K. S., et al. 2007, *Icarus*, 191, 286, doi: [10.1016/j.icarus.2007.04.004](https://doi.org/10.1016/j.icarus.2007.04.004)
- Harris, A. W. 1998, *Icarus*, 131, 291, doi: [10.1006/icar.1997.5865](https://doi.org/10.1006/icar.1997.5865)
- Harris, W., Stern, S. A., & Villanueva, G. L. 2025, in *Centaurs*, ed. K. Volk, M. Womack, & J. Steckloff (IOP Publishing), 16–1—16–26, doi: [10.1088/2514-3433/ada267ch16](https://doi.org/10.1088/2514-3433/ada267ch16)
- Hirabayashi, M., Sánchez, P., & Sarid, G. 2025, in *Centaurs*, ed. K. Volk, M. Womack, & J. Steckloff (IOP Publishing), 12–1—12–30, doi: [10.1088/2514-3433/ada267ch12](https://doi.org/10.1088/2514-3433/ada267ch12)
- Howell, E. S., Magri, C., Vervack, R. J., et al. 2018, *Icarus*, 303, 220, doi: [10.1016/j.icarus.2017.12.003](https://doi.org/10.1016/j.icarus.2017.12.003)
- Hui, M.-T., & Li, J.-Y. 2018, *PASP*, 130, 104501, doi: [10.1088/1538-3873/aad538](https://doi.org/10.1088/1538-3873/aad538)
- Ivezić, Ž., Tabachnik, S., Rafikov, R., et al. 2001, *AJ*, 122, 2749, doi: [10.1086/323452](https://doi.org/10.1086/323452)
- Ivezić, Ž., Lupton, R. H., Jurić, M., et al. 2002, *AJ*, 124, 2943, doi: [10.1086/344077](https://doi.org/10.1086/344077)
- Jewitt, D. 1991, in *Astrophysics and Space Science Library*, Vol. 167, IAU Colloq. 116: *Comets in the post-Halley era*, ed. J. Newburn, R. L., M. Neugebauer, & J. Rahe, 19, doi: [10.1007/978-94-011-3378-4\\_2](https://doi.org/10.1007/978-94-011-3378-4_2)
- Jewitt, D. 2009, *AJ*, 137, 4296, doi: [10.1088/0004-6256/137/5/4296](https://doi.org/10.1088/0004-6256/137/5/4296)
- Jewitt, D. 2021, *AJ*, 161, 261, doi: [10.3847/1538-3881/abf09c](https://doi.org/10.3847/1538-3881/abf09c)
- Johansen, A., Bannister, M., Dones, L., et al. 2025, in *Centaurs*, ed. K. Volk, M. Womack, & J. Steckloff (IOP Publishing), 2–1—2–19, doi: [10.1088/2514-3433/ada267ch2](https://doi.org/10.1088/2514-3433/ada267ch2)
- Kaasalainen, M., & Torppa, J. 2001, *Icarus*, 153, 24, doi: [10.1006/icar.2001.6673](https://doi.org/10.1006/icar.2001.6673)
- Kirchoff, M. R., & Schenk, P. 2010, *Icarus*, 206, 485, doi: [10.1016/j.icarus.2009.12.007](https://doi.org/10.1016/j.icarus.2009.12.007)



- Klahr, H., & Schreiber, A. 2020, *ApJ*, 901, 54, doi: [10.3847/1538-4357/abac58](https://doi.org/10.3847/1538-4357/abac58)
- Kokotanekova, R., Guilbert-Lepoutre, A., Knight, M. M., & Vincent, J. B. 2025, in *Centaurs*, ed. K. Volk, M. Womack, & J. Steckloff (IOP Publishing), 7–1—7–29, doi: [10.1088/2514-3433/ada267ch7](https://doi.org/10.1088/2514-3433/ada267ch7)
- Lacerda, P. 2005, PhD thesis, Leiden Observatory
- Lacerda, P. 2011, *AJ*, 142, 90, doi: [10.1088/0004-6256/142/3/90](https://doi.org/10.1088/0004-6256/142/3/90)
- Lacerda, P., McNeill, A., & Peixinho, N. 2014a, *MNRAS*, 437, 3824, doi: [10.1093/mnras/stt2180](https://doi.org/10.1093/mnras/stt2180)
- Lacerda, P., Fornasier, S., Lellouch, E., et al. 2014b, *ApJL*, 793, L2, doi: [10.1088/2041-8205/793/1/L2](https://doi.org/10.1088/2041-8205/793/1/L2)
- Lamy, P. L., & Toth, I. 1995, *A&A*, 293, L43
- Lamy, P. L., Toth, I., Fernandez, Y. R., & Weaver, H. A. 2004, in *Comets II*, ed. M. C. Festou, H. U. Keller, & H. A. Weaver (Univ. Arizona Press, Tucson, AZ), 223
- Li, J., Jewitt, D., Mutchler, M., Agarwal, J., & Weaver, H. 2020, *AJ*, 159, 209, doi: [10.3847/1538-3881/ab7faf](https://doi.org/10.3847/1538-3881/ab7faf)
- Licandro, J., Hargrove, K., Kelley, M., et al. 2012, *A&A*, 537, A73, doi: [10.1051/0004-6361/201118142](https://doi.org/10.1051/0004-6361/201118142)
- Lineweaver, C. H., & Norman, M. 2010, arXiv e-prints, arXiv:1004.1091, doi: [10.48550/arXiv.1004.1091](https://doi.org/10.48550/arXiv.1004.1091)
- Lisse, C. M., Fernández, Y. R., Kundu, A., et al. 1999, *Icarus*, 140, 189, doi: [10.1006/icar.1999.6131](https://doi.org/10.1006/icar.1999.6131)
- Liu, P.-Y., & Ip, W.-H. 2019, *ApJ*, 880, 71, doi: [10.3847/1538-4357/ab29eb](https://doi.org/10.3847/1538-4357/ab29eb)
- Luu, J., & Jewitt, D. 1996, *AJ*, 112, 2310, doi: [10.1086/118184](https://doi.org/10.1086/118184)
- Luu, J. X., & Jewitt, D. C. 1990, *AJ*, 100, 913, doi: [10.1086/115571](https://doi.org/10.1086/115571)
- Luu, J. X., & Jewitt, D. C. 1998, *ApJL*, 494, L117, doi: [10.1086/311172](https://doi.org/10.1086/311172)
- Mainzer, A. K., Bauer, J. M., Cutri, R. M., et al. 2019, NASA Planetary Data System, doi: [10.26033/18S3-2Z54](https://doi.org/10.26033/18S3-2Z54)
- Mainzer, A. K., Masiero, J. R., Abell, P. A., et al. 2023, *PSJ*, 4, 224, doi: [10.3847/PSJ/ad0468](https://doi.org/10.3847/PSJ/ad0468)
- Mandt, K., Ivanova, O., Harrington Pinto, O., Roth, N. X., & Seligman, D. Z. 2025, in *Centaurs*, ed. K. Volk, M. Womack, & J. Steckloff (IOP Publishing), 6–1—6–34, doi: [10.1088/2514-3433/ada267ch6](https://doi.org/10.1088/2514-3433/ada267ch6)
- Mann, R. K., Jewitt, D., & Lacerda, P. 2007, *AJ*, 134, 1133, doi: [10.1086/520328](https://doi.org/10.1086/520328)
- Marschall, R., Morbidelli, A., Bottke, W. F., et al. 2023, in *Asteroids, Comets, Meteors Conference 2023*, 2470
- Marschall, R., Nesvorný, D., Deienno, R., et al. 2022, *AJ*, 164, 167, doi: [10.3847/1538-3881/ac8d6b](https://doi.org/10.3847/1538-3881/ac8d6b)
- McKinnon, W. B., Richardson, D. C., Marohnic, J. C., et al. 2020, *Science*, 367, aay6620, doi: [10.1126/science.aay6620](https://doi.org/10.1126/science.aay6620)
- McNeill, A., Fitzsimmons, A., Jedicke, R., et al. 2018, *AJ*, 156, 282, doi: [10.3847/1538-3881/aaeb8c](https://doi.org/10.3847/1538-3881/aaeb8c)
- Mommert, M., Jedicke, R., & Trilling, D. E. 2018, *AJ*, 155, 74, doi: [10.3847/1538-3881/aaa23b](https://doi.org/10.3847/1538-3881/aaa23b)
- Morgado, B. E., Sicardy, B., Braga-Ribas, F., et al. 2021, *A&A*, 652, A141, doi: [10.1051/0004-6361/202141543](https://doi.org/10.1051/0004-6361/202141543)
- Mottola, S., Britt, D. T., Brown, M. E., et al. 2024, *SSRv*, 220, 17, doi: [10.1007/s11214-024-01052-7](https://doi.org/10.1007/s11214-024-01052-7)
- Mottola, S., Hellmich, S., Buie, M. W., et al. 2023, *PSJ*, 4, 18, doi: [10.3847/PSJ/aca7f9](https://doi.org/10.3847/PSJ/aca7f9)
- Müller, T., Lellouch, E., & Fornasier, S. 2020, in *The Trans-Neptunian Solar System*, ed. D. Prialnik, M. A. Barucci, & L. Young, 153–181, doi: [10.1016/B978-0-12-816490-7.00007-2](https://doi.org/10.1016/B978-0-12-816490-7.00007-2)
- Myers, S. A., Howell, E. S., Magri, C., et al. 2023, *PSJ*, 4, 5, doi: [10.3847/PSJ/aca89d](https://doi.org/10.3847/PSJ/aca89d)
- Namouni, F., & Morais, M. H. M. 2020, *MNRAS*, 494, 2191, doi: [10.1093/mnras/staa712](https://doi.org/10.1093/mnras/staa712)
- Nesvorný, D. 2018, *ARA&A*, 56, 137, doi: [10.1146/annurev-astro-081817-052028](https://doi.org/10.1146/annurev-astro-081817-052028)
- Nesvorný, D. 2021, *ApJL*, 908, L47, doi: [10.3847/2041-8213/abe38f](https://doi.org/10.3847/2041-8213/abe38f)
- Nesvorný, D., Vokrouhlický, D., Bottke, W. F., & Levison, H. F. 2018, *Nature Astronomy*, 2, 878, doi: [10.1038/s41550-018-0564-3](https://doi.org/10.1038/s41550-018-0564-3)
- Nesvorný, D., Vokrouhlický, D., Alexandersen, M., et al. 2020, *AJ*, 160, 46, doi: [10.3847/1538-3881/ab98fb](https://doi.org/10.3847/1538-3881/ab98fb)
- Noll, K. S., Grundy, W. M., Stephens, D. C., Levison, H. F., & Kern, S. D. 2008, *Icarus*, 194, 758, doi: [10.1016/j.icarus.2007.10.022](https://doi.org/10.1016/j.icarus.2007.10.022)
- Noll, K. S., Levison, H. F., Grundy, W. M., & Stephens, D. C. 2006, *Icarus*, 184, 611, doi: [10.1016/j.icarus.2006.05.010](https://doi.org/10.1016/j.icarus.2006.05.010)

- Ortiz, J. L., Duffard, R., Pinilla-Alonso, N., et al. 2015, *A&A*, 576, A18, doi: [10.1051/0004-6361/201424461](https://doi.org/10.1051/0004-6361/201424461)
- Peixinho, N., Delsanti, A., Guilbert-Lepoutre, A., Gafeira, R., & Lacerda, P. 2012, *A&A*, 546, A86, doi: [10.1051/0004-6361/201219057](https://doi.org/10.1051/0004-6361/201219057)
- Peixinho, N., Lilly, E., Alvarez-Candal, A., Souza-Feliciano, A. C., & Seccull, T. 2025, in *Centaurs*, ed. K. Volk, M. Womack, & J. Steckloff (IOP Publishing), 5–1—5–18, doi: [10.1088/2514-3433/ada267ch5](https://doi.org/10.1088/2514-3433/ada267ch5)
- Peixinho, N., Thirouin, A., Tegler, S. C., et al. 2020, in *The Trans-Neptunian Solar System*, ed. D. Prialnik, M. A. Barucci, & L. Young (Elsevier), 307–329, doi: [10.1016/B978-0-12-816490-7.00014-X](https://doi.org/10.1016/B978-0-12-816490-7.00014-X)
- Porter, S. B., Benecchi, S. D., Verbiscer, A. J., et al. 2024, *PSJ*, 5, 143, doi: [10.3847/PSJ/ad3f19](https://doi.org/10.3847/PSJ/ad3f19)
- Pravec, P., & Harris, A. W. 2007, *Icarus*, 190, 250, doi: [10.1016/j.icarus.2007.02.023](https://doi.org/10.1016/j.icarus.2007.02.023)
- Ruprecht, J. D., Bosh, A. S., Person, M. J., et al. 2015, *Icarus*, 252, 271, doi: [10.1016/j.icarus.2015.01.015](https://doi.org/10.1016/j.icarus.2015.01.015)
- Safrit, T. K., Steckloff, J. K., Bosh, A. S., et al. 2021, *PSJ*, 2, 14, doi: [10.3847/PSJ/abc9c8](https://doi.org/10.3847/PSJ/abc9c8)
- Samarasinha, N. H., & Mueller, B. E. A. 2013, *ApJL*, 775, L10, doi: [10.1088/2041-8205/775/1/L10](https://doi.org/10.1088/2041-8205/775/1/L10)
- Schäfer, U., Yang, C.-C., & Johansen, A. 2017, *A&A*, 597, A69, doi: [10.1051/0004-6361/201629561](https://doi.org/10.1051/0004-6361/201629561)
- Schenk, P. M., Chapman, C. R., Zahnle, K., & Moore, J. M. 2004, in *Jupiter. The Planet, Satellites and Magnetosphere*, ed. F. Bagenal, T. E. Dowling, & W. B. McKinnon, Vol. 1 (Cambridge University Press), 427–456
- Schwamb, M. E., Jones, R. L., Yoachim, P., et al. 2023, *ApJS*, 266, 22, doi: [10.3847/1538-4365/acc173](https://doi.org/10.3847/1538-4365/acc173)
- Sheppard, S. S., & Jewitt, D. 2004, *AJ*, 127, 3023, doi: [10.1086/383558](https://doi.org/10.1086/383558)
- Showalter, M. R., Benecchi, S. D., Buie, M. W., et al. 2021, *Icarus*, 356, 114098, doi: [10.1016/j.icarus.2020.114098](https://doi.org/10.1016/j.icarus.2020.114098)
- Sickafoose, A., Giuliatti Winter, S. M., Leiva, R., et al. 2025, in *Centaurs*, ed. K. Volk, M. Womack, & J. Steckloff (IOP Publishing), 9–1—9–31, doi: [10.1088/2514-3433/ada267ch9](https://doi.org/10.1088/2514-3433/ada267ch9)
- Simon, J. B., Armitage, P. J., Li, R., & Youdin, A. N. 2016, *ApJ*, 822, 55, doi: [10.3847/0004-637X/822/1/55](https://doi.org/10.3847/0004-637X/822/1/55)
- Singer, K. N., McKinnon, W. B., Gladman, B., et al. 2019, *Science*, 363, 955, doi: [10.1126/science.aap8628](https://doi.org/10.1126/science.aap8628)
- Spoto, F., Milani, A., & Knežević, Z. 2015, *Icarus*, 257, 275, doi: [10.1016/j.icarus.2015.04.041](https://doi.org/10.1016/j.icarus.2015.04.041)
- Steckloff, J. K., & Samarasinha, N. H. 2018, *Icarus*, 312, 172, doi: [10.1016/j.icarus.2018.04.031](https://doi.org/10.1016/j.icarus.2018.04.031)
- Stern, S. A., Weaver, H. A., Spencer, J. R., et al. 2019, *Science*, 364, aaw9771, doi: [10.1126/science.aaw9771](https://doi.org/10.1126/science.aaw9771)
- Tegler, S. C., Romanishin, W., Consolmagno, G. J., & J., S. 2016, *AJ*, 152, 210, doi: [10.3847/0004-6256/152/6/210](https://doi.org/10.3847/0004-6256/152/6/210)
- Tegler, S. C., Romanishin, W., Consolmagno, G. J., et al. 2005, *Icarus*, 175, 390, doi: [10.1016/j.icarus.2004.12.011](https://doi.org/10.1016/j.icarus.2004.12.011)
- Thébault, P. 2003, *Earth Moon and Planets*, 92, 233, doi: [10.1023/B:MOON.0000031941.77871.c5](https://doi.org/10.1023/B:MOON.0000031941.77871.c5)
- Thirouin, A., & Sheppard, S. S. 2018, *AJ*, 155, 248, doi: [10.3847/1538-3881/aac0ff](https://doi.org/10.3847/1538-3881/aac0ff)
- Vokrouhlický, D., Nesvorný, D., Bottke, W. F., & Morbidelli, A. 2010, *AJ*, 139, 2148, doi: [10.1088/0004-6256/139/6/2148](https://doi.org/10.1088/0004-6256/139/6/2148)
- Volk, K., & Malhotra, R. 2008, *ApJ*, 687, 714, doi: [10.1086/591839](https://doi.org/10.1086/591839)
- Volk, K., Womack, M., & Steckloff, J. 2025, in *Centaurs*, ed. K. Volk, M. Womack, & J. Steckloff (IOP Publishing), 1–1—1–17, doi: [10.1088/2514-3433/ada267ch1](https://doi.org/10.1088/2514-3433/ada267ch1)
- Warner, B. D., Harris, A. W., & Pravec, P. 2009, *Icarus*, 202, 134, doi: [10.1016/j.icarus.2009.02.003](https://doi.org/10.1016/j.icarus.2009.02.003)
- Wong, I., & Brown, M. E. 2015, *AJ*, 150, 174, doi: [10.1088/0004-6256/150/6/174](https://doi.org/10.1088/0004-6256/150/6/174)
- Wong, I., & Brown, M. E. 2017, *AJ*, 153, 145, doi: [10.3847/1538-3881/aa60c3](https://doi.org/10.3847/1538-3881/aa60c3)
- Wright, E., Mainzer, A., Masiero, J., et al. 2018, *arXiv e-prints*, arXiv:1811.01454, doi: [10.48550/arXiv.1811.01454](https://doi.org/10.48550/arXiv.1811.01454)
- Wright, E. L. 2007, *arXiv e-prints*, astro, doi: [10.48550/arXiv.astro-ph/0703085](https://doi.org/10.48550/arXiv.astro-ph/0703085)
- Yoshida, F., & Terai, T. 2017, *AJ*, 154, 71, doi: [10.3847/1538-3881/aa7d03](https://doi.org/10.3847/1538-3881/aa7d03)



Zahnle, K., Schenk, P., Levison, H., & Dones, L.  
2003, *Icarus*, 163, 263,  
doi: [10.1016/S0019-1035\(03\)00048-4](https://doi.org/10.1016/S0019-1035(03)00048-4)